Interaction Mechanism of Modified Collagen-Binding Antimicrobial Peptide LL37 with Model Lipid Bilayers

A Major Qualifying Project

Submitted to the Faculty
of
Chemical Engineering
Worcester Polytechnic Institute

In Partial Fulfillment of the Requirements for the
Degree of Bachelor of Science

Yoon Kyong Lee, CHE
Rachel Elizabeth Smith, CHE

April 27, 2017

Submitted to:

Professor Terri Camesano, Advisor

Acknowledgments

First, we would like to thank our advisor, Professor Terri A. Camesano for providing us with his interesting and informative Major Qualifying Project (MQP). We are grateful for her continuous guidance and support throughout this project.

We would like to thank PhD candidate Lindsay Lozeau for her assistance with lab training. Finally, we would like to thank everyone that has been accommodating to us in the Camesano Lab. Thank you for making us feel welcome in the lab and assisting us wherever they could.

Abstract

Antibiotic-resistant bacteria and chronic wound infections pose a serious threat to patient health and overall quality of life. The goal of this project was to determine the action mechanism of *f*CBD-LL37 against phosphatidylcholine lipid bilayer using a quartz crystal microbalance with dissipation. At increased concentrations, *f*CBD interacted to a greater extent with the lipid bilayer indicating that the tethered *f*CBD-LL37 shows greater peptide bondage to bilayer. This is the foundation of the development of bipolymer-tethered AMPs for wound healing applications.

Table of Contents

Table of Figures

Chapter 1: Introduction

Chronic wound infections pose a serious threat to patient health and overall quality of life, and billions of dollars are spent in the United States each year for chronic wound treatments. Current approaches to mitigate them such as antibiotics and silver are becoming increasingly ineffective because of bacterial resistance and inhibition of healing. Thus, there is a pressing need for alternative approaches that treat wound infections and also facilitate functional tissue repair (Center of Disease Control, 2016).

Antimicrobial peptides (AMPs) are a promising alternative treatment because of their broad-spectrum antimicrobial activities. AMPs are short, naturally-occurring peptides that display a generally physical mechanisms of membrane disruption (Wang, 2016). This allows for antimicrobial activity against antibiotic-resistant organisms and a low chance for the development of resistance. Many AMPs, such as the human LL37 have additional immunomodulatory activities that are attractive as wound treatments (Lozeau, Grosha, Kole, Prifti, Dominko, Camesano, Rolle, 2016). There are over 2,600 natural AMPs that could be utilized as a diverse platform for the development of new antimicrobial agents, as well as, target antibiotic-resistant agents (Center of Disease Control, 2016). However, due to their cytotoxicity at high concentrations, more research must be done prior to their clinical use to improve their therapeutic index for preventing infection wound healing applications.

Targeted delivery of AMPs bound to collagen scaffolds may broaden AMP technologies for clinical wound healing application (Lozeau et al, 2016). Collagen is a prevalent biopolymer in repairing tissues and commercially available wound dressings (Lozeau, Grosha, Kole, Prifti, Dominko, Camesano, Rolle, 2016). Although several prior studies have explored tethering of AMPs, the tethering of AMPs with biopolymers such as

collagen remain unknown (Lozeau, Grosha, Kole, Prifti, Dominko, Camesano, Rolle, 2016). Previously, two modified versions of the human LL37 were designed with collagen-binding domains (CBDs) and studied for their collagen-binding and bioactivity (Lozeau et al, 2016); however, it is unknown whether adding CBD alters LL37's mechanism of interaction with membranes.

The overall goal of this project is to determine the action mechanism of one of these CBD peptides, *f*CBD-LL37 with a CBD derived from fibronectin, against zwitterionic phosphatidylcholine (PC) lipid bilayers. We chose to study fCBD-LL37 because from prior research, it is found that fCBD is less cytotoxic and preserves its antimicrobial activity. To do this, we used the quartz-crystal microbalance with dissipation (QCM-D) to develop a better understanding for the molecular basis of *f*CBD-LL37 mechanisms as a function of concentration (Wang, 2015). The obtained frequency (Δf) and (ΔD) values were analyzed in terms of time, overall changes, and molecular fingerprint at the different peptide-to-lipid ratios (P/L). From this, we were able to develop a hypothesis for the action mechanism of *f*CBD-LL37 as a function of concentration. These studies will allow us to observe how adding *f*CBD affected LL37 bioactivity, provide a foundation for future research, and aid in the development of biopolymer-tethered AMPs for wound healing applications.

Chapter 2: Literature Review

I. The Antimicrobial Resistance Crisis

The number of infections caused by multidrug-resistant bacteria is increasing due to high use and reliance on antibiotics (Center of Disease Control, 2014). It is estimated that in the United States, 2 million people are infected with antibiotic-resistant bacteria annually that results in approximately 23,000 deaths (Blair, Webber, Baylay, Ogbolu, Piddock, 2015).

Resistance can occur by many routes, and new resistance mechanisms are constantly being described (Blair, Webber, Baylay, Ogbolu, Piddock, 2015). Mechanisms such as antibiotic control programs, better hygiene, and synthesis of agents with improved antimicrobial activity need to be adopted in order to limit bacterial resistance (Neu H, 1992). Unfortunately, the approval of alternative antimicrobial agents has been dwindling. This is particularly a problem in situations where alternatives such as silver or chemicals should not be used, such as in chronic wounds.

II. Chronic Wounds

Wound healing is an essential process for the repair and restoration of function tissue after injury. After a wound is infected, healing begins with inflammation, is followed by a period of tissue regeneration including epithelialization, angiogenesis and ends with remodeling to restore the tissue (Mangoni, McDermott, Zasloff, 2015). A wound that does not heal in an orderly set of stages and in a predictable amount of time can lead to the formation of non-healing chronic wounds (Mangoni, McDermott, Zasloff, 2015). Chronic wounds (such as ulcers, burns and surgical site infections) represent a significant burden to patients and healthcare professionals, affecting approximately 5.7 million patients and costing approximately $20 billion annually (Torre, 2015). Typically, antimicrobial agents

are used during wound treatment to mitigate the chance of infection in addition to the use of wound scaffolds that help the functional tissue repair.

The Use of Scaffolds for Chronic Wound Treatment

Recent advances in our understanding of chronic wound biology have led to the development of several new treatments that offer renewed hope to patients with ulcers and other chronic wounds. Factors underlying the wound healing problems experienced in individual patients should allow better tailored treatment to each individual. Allogeneic skin grafting (transplanted between people who are not genetically identical) and bioengineered skin equivalents are being used successfully in patients with venous leg ulcers and diabetic patients with foot ulcers (Morris, Patel, 2002). Bioengineered skin consists of an outer epidermal layer and/or a dermal layer (the layer of skin between the epidermis and the subcutaneous tissue) embedded into an acellular matrix (a support structure) forming a biological skin substitute (Ranaweera, 2011). Bioengineered skin graft Alloderm is currently being used for burn and full thickness wounds (Ranaweera, 2011). Skin tissue donated from cadavers are used to make an acellular dermal matrix that has been freeze-dried after processing. It is used to serve as a scaffold for normal tissue remodeling (Ranaweera, 2011). The collagen framework provides strength to the skin and contains no cells that can cause rejection or irritation (Ranaweera, 2011).

Despite the growing number of new wound dressings and therapeutics, current scientific data is incomplete, and evidence for the effectiveness of these wound dressings combined with antimicrobial treatment is sparse. A combination approach of wound-care management (debridement and scaffolding), systemic antibiotics, and a topical antimicrobial agent has been shown to reduce the ability of the infection to persist (Wolcott and Rhoads, 2008; Lopez-Leban et al., 2010; Wolcott et al., 2010) and has been shown to be one effective approach to healing these wounds. Unfortunately, these multifaceted treatments can also be costly. Alternatively, silver dressings are used to prevent infection,

but it is scrutinized for its inability to promote healing (Castellano, Shafii, Ko, Donate, Wright, Mannari, Payne, Smith, 2007). No significant advantage of one wound dressing over the other currently exists which increases the chance of wounds being more likely to be infected (Vasa, 2013).

Chronic Wound Infection

Chronic wounds are highly susceptible to infection, which severely complicates treatment, these wounds are also expensive to treat costing about $25 billion annually on treat (Sen, Gordillo, Roy, Kirsner, Lambert, Hunt, Gottrup, Gurtner, Longaker, 2009). When there is infection, various bacteria may form biofilms on the wound surface, which are characterized by an aggregation of bacterial cells immobilized in an impenetrable adhesive matrix made of extracellular polymeric substances. Biofilms make the eradication of bacteria difficult, mainly due to the weak penetration of antibiotics or host clearance mechanisms (Mangoni, McDermott, Zasloff, 2015). Wound infections are currently treated with antibiotics, such as aminoglycosides (see **Appendix A** for list of common antibiotics). Using antibiotics unnecessarily or incorrectly increases the risk of bacteria developing resistance to antibiotics. Furthermore, many wounds are polymicrobial (consisting of many bacterial species), which are difficult for antibiotics to target. There is a need for new ways to avoid bacterial resistance, combat polymicrobial infection, and help heal chronic wounds.

III. Antimicrobial Peptides are a Promising Alternative

Antimicrobial peptides (AMPs) have shown promise in helping with the antibiotic resistance crisis and the treatment of chronic wounds. AMPs are small molecular weight proteins with the broad-spectrum antimicrobial activity against bacteria, viruses and fungi. They are usually positively-charged (net charge between −3 and +20) (Wang, G 2014). They also are amphipathic, and have both hydrophobic and hydrophilic residues that enable

the molecule to be soluble in both aqueous environments and lipid-rich membranes (Wang, G 2014). The unique physical interaction mechanisms of AMPs with lipid membranes lead to a lower likelihood to bacterial resistance, making AMPs highly promising for the clinic. However, despite significant progress in the past 30 years, no peptide antibiotic has reached the clinic yet. Poor understanding of the action mechanisms and lack of rational design principles have been the two major obstacles that have slowed progress (Li, Koh, Liu, Lakshminarayanan, Verma, Beuerman, 2017). AMPs also have a high production cost estimated at $300-$500 per gram (Bray 2003; Vlieghe et al. 2010). These shortcomings could be improved with a better understanding of the exact mechanisms of AMP interactions, because then, alternative and less toxic designs of AMPs could be designed.

IV. Human Cathelicidin AMP LL37

Cathelicidins are a family of mammalian AMPs found in the granules of neutrophils and are synthesized as preproproteins. After removal of a signal peptide, they are stored in granules as inactive proforms. The active biologic domains of the cathelicidins reside in the C-terminus, with the N-terminus having a conserved cathelin-like domain. Commonly studied examples of cathelicidins including ovine SMAP-29, bovine indolicidin, and porcine PR-39 (Wang K, 2015).

The only human-derived cathelicidin is LL37, a 37-aa protein (see LL37 sequence in **Figure 1**). LL37 demonstrates broad antimicrobial, anti-biofilm and immunomodulatory activities. Fifty-four percent of LL37's residues are hydrophilic with 11 basic and 5 acidic, giving it a net positive charge of +6 at physiological pH. In aqueous solution, LL37 has a disordered structure, but when exposed to a lipophilic environment, many of the amino acids are able to form intramolecular hydrogen bonds locking the secondary structure into an α-helix (Duplantier, van Hoek, 2013). When administered topically, can potentially avoid the many hurdles of systemic peptide delivery (Duplantier, van Hoek, 2013). An

intriguing aspect of LL-37 with respect to skin wounds is its interaction with keratinocytes. Keratinocytes, the predominant cell type found in the epidermis, form barriers against microbial pathogens during wound closure, and keratinocyte migration is an important step in skin wound healing (Duplantier, van Hoek, 2013). hCAP-18 is strongly expressed in healing skin epithelium, and treatment with antibodies raised and affinity purified against LL-37 inhibited re-epithelialization (wound closure) in a concentration-dependent manner (Heilborn et al., 2003). However, action mechanisms of LL37 are not fully understood to start using clinical applications. The combination of the anti-biofilm and pro-wound healing properties of LL37 may make it highly effective in resolving polymicrobial-infected wounds, which could make it an excellent alternative therapeutic for chronic wounds.

LL37 Modified to Bind to Collagen-Based Materials

In order to mitigate cytotoxicity and maintain activity while delivering LL37 to a wound site, research was done to investigate the effects of tethering human AMP cathelicidin LL37 to collagen. Collagen is one of the main extracellular matrix proteins in wound sites, and in commercially-available wound dressings. The active domain of LL37 was modified by fusion to two different collagen binding domains (CBD) (see **Figure 1** for CBDs), one from derived from collagenase (*c*CBD-LL37) and one derived from fibronectin (*f*CBD-LL37) (Lozeau, Grosha, Kole, Prifti, Dominko, Camesano, Rolle, 2016). This study found that *f*CBD-LL37 is less cytotoxic in solution than *c*CBD-LL37 and LL37 and the biopolymer-tethered AMPs may represent a viable alternative for preventing and treating wound infection while also supporting tissue repair.

Given the unique, non-toxic action of *f*CBD-LL37 from this recent study in particular, we were interested in the interaction mechanisms of *f*CBD-LL37 with zwitterionic mammalian cell membranes and the role that *f*CBD plays in that mechanism. There are many possible mechanisms that AMPs could adopt when faced with zwitterionic lipid membranes.

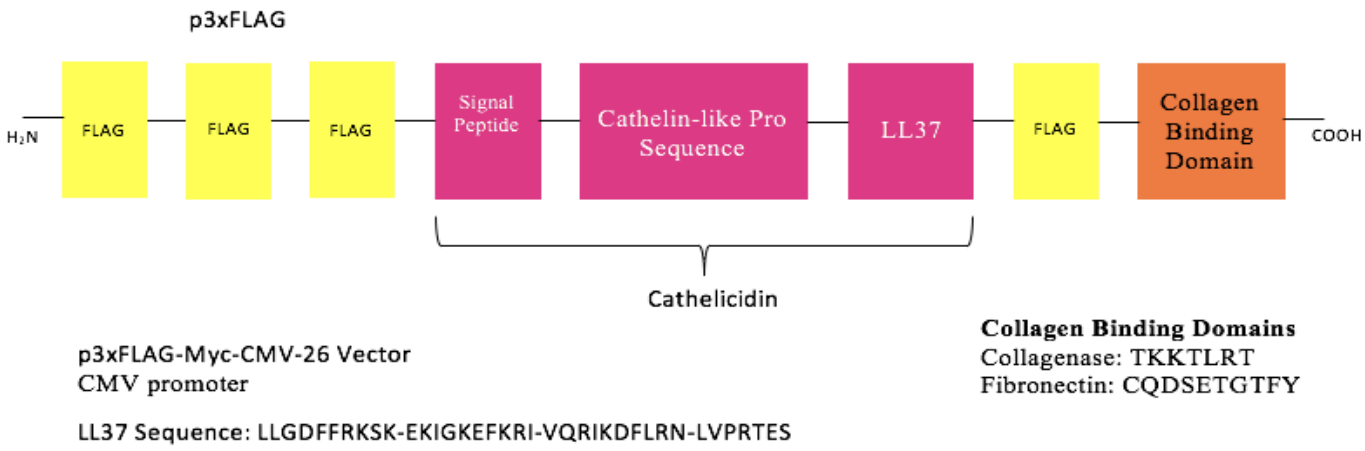

Figure 1:Full structure of cCBD-LL37 and fCBD-LL37 precursors taken from (Prifti, 2012). The AMP includes three FLAG domains and the cathelin-like signal and pro-sequences, all of which are cleaved after cellular secretion, leaving the LL37 active domain (magenta), one FLAG sequence as a spacer and identifiable sequence (yellow) and the collagen binding domain (orange).

V. Proposed AMP-Lipid Interaction Mechanisms

The overall mechanism of AMPs is determined their ability to cause damage to cell membranes. The composition of the cell membrane plays a role in determining the potency and specificity of AMPs. The sensitivity of the bacterial and mammalian cells to AMPs is directly mediated by the physicochemical properties of the lipids found in each type of membrane (Dathe and Wieprecht, 1999). Indeed, the negative charge of bacterial

membranes (anionic lipids for example phosphatidylglycerol and cardiolipin) is important for preferential binding of some AMPs, including LL37, to microorganisms. This interaction is governed by electrostatic interactions between cationic AMPs and anionic bacterial membranes.

When encountering zwitterionic lipids (such as phosphatidylcholine), then there are relatively weaker attractive interactions between neutral membranes and AMPs (Wang, 2014). In this case, hydrophobicity may be more significant in determining activity. Hydrophobicity has been shown to affect the antimicrobial and hemolytic activity of AMPs (Wang, 2014). Numerous studies have examined the relationship between many AMPs' structures and their resulting bioactivities. However, in the case of LL37, its structure, physicochemical properties and mechanisms of cytotoxicity are still controversial. It is generally agreed upon that for LL37, its mechanism depends on several properties such as peptide-to-lipid ratio (P/L), charge, sequence and secondary structure orientation and aggregation (Guilhelmelli, *et al.*, 2013). Several models relating these properties have been proposed (**Figure 2**).

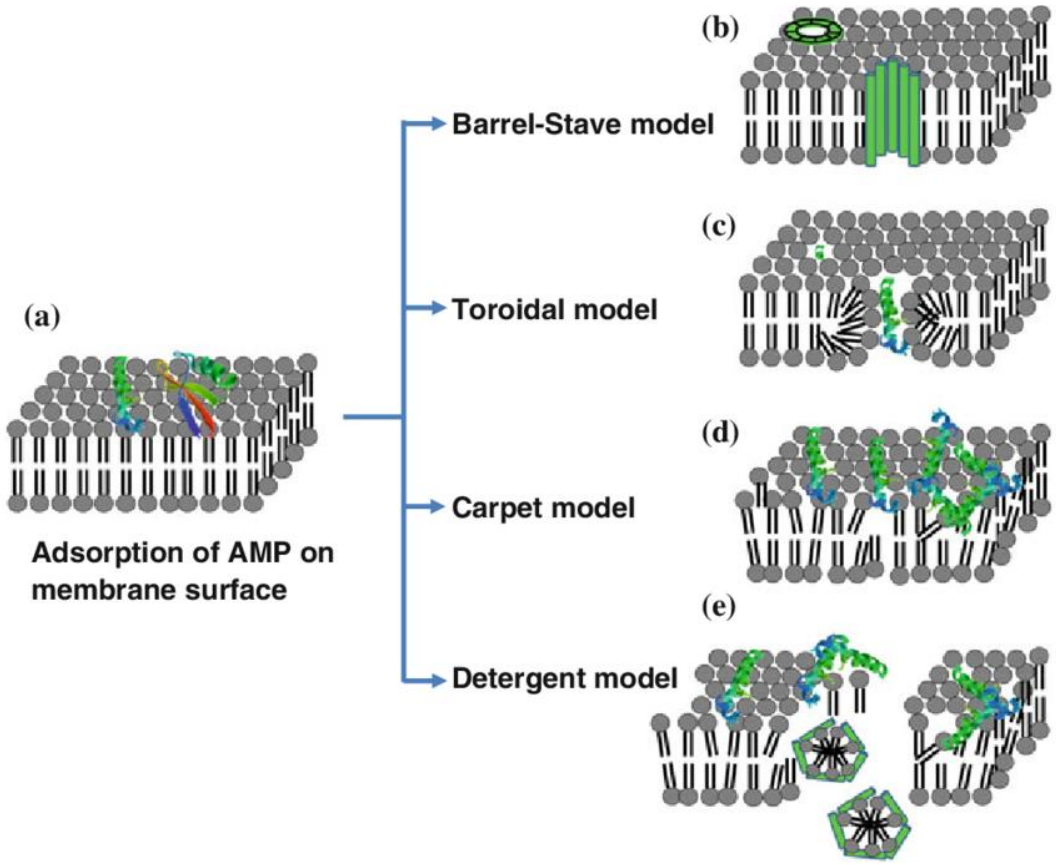

Figure 2:Commonly cited models for antimicrobial peptide activity. Figure 2a represents the adsorption of AMP on the membrane surface, Figure 2b represents the Barrel-stave Pore mechanism, Figure 2c represents Torodial Pore mechanism, Figure 2d represents the Carpet Model and Figure 2e represents the Detergent Model. Barrel-stave and toroidal pores are membrane-spanning aqueous channels. Antimicrobial peptides are described with the carpet model. Such peptides permeabilize membranes by "carpeting" the bilayer. Picture adapted from Academic paper: Plant Antimicrobial Peptides. Available from: https://www.researchgate.net/publication/302072901_Plant_Antimicrobial_Peptides [accessed Mar 31, 2017]

The proposed models for AMP mechanisms include the toroidal pore, barrel-stave, non-pore carpet, and detergent-like carpet models (see **Figure 2**). The exact mechanism that LL37 adopts against zwitterionic membranes is still not clearly understood. In fact, many different mechanisms have been proposed, including the toroidal pore, non-pore carpet, and detergent-like carpet mechanisms. It is possible that *f*CBD-LL37 follows similar or vastly different mechanisms than LL37, mediated by its unique CBD.

In the toroidal model, AMPs are inserted into the membrane forming a bundle, inducing the lipid monolayers to continuously bend through the pore (Yang et al., 2001) (**Figure 2c**). This is often dependent on AMP aggregation. As a result, the membrane lipids become interspersed with AMPs (Yeaman & Yount, 2003). An important aspect of this mechanism involves an induction of positive curvature strain in the bilayer by the AMP at high concentrations, leading to the formation of small and transient lipid-AMP pores (Wildman, Lee, & Ramamoorthy, 2002). LL37 was shown to do this, using NMR spectroscopy, in PE lipid bilayers that typically favor negative curvature (Wildman, Lee, Ramamoorthy, 2002). Other examples of AMPs that form toroidal pores are magainins, protegrins, and melittin (Brogden, 2005).

In a barrel stave pore (**Figure 2b)**, peptides interact laterally with one another to form a specific structure that is reminiscent of a membrane protein ion channel. Barrel stave pores work with the bilayer hydrocarbon core, using it as a template for peptide-self assembly (Wimley, 2011). Additional monomers can increase the pore size, allowing cytoplasmic content leaking with subsequent cell death. In this mechanism, peptide secondary structures, such as hydrophobic α-helix and/or β-sheet, are essential to pore formation (Breukink and de Kruijff, 1999). These peptide regions interact with the membrane lipids, while the hydrophilic peptide regions form the lumen of the channel (Brogden, 2005).

In the non-pore carpet model (**Figure 2c**), AMPs align themselves parallel to membrane surface, facilitated by their amphipathicity. The AMPs must first bind onto the surface of the target membrane, possibly in monomeric form, and cover it in a "carpet"-like manner (Oren Z., Shai Y, 2001). Initial interaction is driven by electrostatics in the case of anionic lipids, and amphipathicity in the case of zwitterionic lipids. When the amount of AMPs on the membrane surface reaches a critical threshold concentration, the

membrane is permeated, wholly disrupted, and is disintegrated at the highest AMP concentrations (Oren and Shai, 1998). The threshold concentration (denoted as P/L*) depends upon the composition of lipid membrane. Well-defined pores do not occur in this model. A study was done to investigate the the active conformation in the membranes of LL37 by reconstituting LL37 into nto dodecylphosphocholine (DPC) micelles and determine its 3D structure (Porcelli *et al.,* 2008). It was found that under experimental conditions the peptide adopts a helix-break-helix conformation (Porcelli *et al.*, 2008). When it interacts with DPC, LL-37 is adsorbed on the surface of the micelle with the hydrophilic face exposed to the water phase and the hydrophobic face buried in the micelle hydrocarbon region. These results support the proposed nonpore carpet-like mechanism of action, in agreement with the solid-state NMR studies (Porcelli *et al.*, 2008).

In detergent-like carpet model (**Figure. 2e**), AMPs surround the lipids and carpet on the surface as they do in the non-pore carpet mechanism. However, at P/L*, peptide-lipid micelles break off from the lipid membrane, causing large defects in the membrane, lysis and cell death. A detergent-like mechanism, was rated unlikely to be the mechanism of LL37 because of the rapidly tumbling membrane fragments that were not observed in NMR experiments carried out (Sevcsik *et al.,* 2007). This dual behavior of LL-37 can be attributed to a balance between electrostatic interactions reflected in different penetration depths of the peptide and hydrocarbon chain length. This study indicates that there is a tight coupling between the peptide properties and those of the lipid bilayer, which needs to be considered in studies of lipid/peptide interaction (Sevcsik *et al.*, 2007). In extension to these studies observations on PG and PC model membranes clearly demonstrate that the peptide LL-37 does not act by one single molecular mechanism, but causes membrane disruption by distinctly different mechanisms strongly dependent not only on the nature of the lipid headgroup but also on the hydrocarbon chain length (Sevcsik *et al.,* 2007).

However, it has been described that AMPs might also form transmembrane pores

at concentrations below the threshold, suggesting that the mechanism by which the peptide disrupts the membrane depends on its concentration (Lohner, 2009). It is possible that derivatives of LL37 such as *f*CBD-LL37 have similar mechanisms; however, the low toxicity of *f*CBD-LL37 compared with LL37 alone suggests that these mechanisms may deviate particularly in the case of zwitterionic membranes. Further, the structure of *f*CBD-LL37 may cause alternate conformations on the lipid surface leading to different outcomes for interaction mechanisms. It was suggested previously that *f*CBD-LL37 may aggregate, thus helping to lower its toxicity.

VI. QCM-D: A Method to Elucidate fCBD-LL37 Mechanism

Quartz crystal microbalance with dissipation (QCM-D) is a versatile technique for investigating AMPs. QCM-D measures a mass variation per unit area by measuring the change in frequency (Δf) of a piezoelectric quartz crystal resonator. The added advantage of measuring dissipation (ΔD) changes allows additional film properties to be investigated (Dixon M, 2008). ΔD is related to the rigidity of the film. The QCM-D measures these responses for various overtones, or multiples of the resonant frequency (5 MHz). Overtones can be correlated with the changes in depths of a film deposited on the crystal (Dixon M, 2008). The QCM-D is a non-destructive flow system, which allows all of these changes to be measured in real-time, giving more information about interaction mechanisms than spectroscopic systems, which are both destructive and limited to one point in time during the interaction. The use of QCM-D for experiments is promising for the differentiation of peptide mechanisms.

QCM-D can give information about mass deposition, changes in bilayer integrity the dynamics of AMP–membrane interactions (Dixon, 2008). Previously, AMP mechanisms were investigated versus zwitterionic phosphatidylcholine (PC) lipid bilayers (Wang, 2015). A bilayer was formed in the QCM-D, and varying concentrations of AMP were injected through the system. From the changes in ΔD and Δf, mechanisms were

proposed. For example, Indolicidin, a 13-residue bovine cathelicidin that assumes a unique folded conformation when in contact with PC (Wang, 2015), was found to create substantial changes in the PC membranes at concentrations above 1 μM in the QCM-D experiments that correlated with the Minimum Inhibitory Concentration (MIC) of 1 to 13 μM for various bacteria and hemolytic concentrations (Wang, 2015). Even more information about AMP mechanisms were found by further analysis of the raw data in polar plot form (ΔD vs. Δf). Using polar plots, the unique fingerprint for indolicidin's mechanism was compared to three other AMPs, and allowed differentiation of the phenomena directly occurring at bilayer during AMP-PC interaction. This gave more insight to the interaction than simple ΔD and Δf changes alone.

Our goal to determine the action mechanism of chimeric *f*CBD-LL37 against PC bilayers using QCM-D as a function of peptide concentration to develop a better understanding for the molecular basis of *f*CBD-LL37 mechanisms. We investigated the initial and overall interactions of *f*CBD-LL37 with PC over time at different concentrations. Polar plots were constructed to create a unique fingerprint for *f*CBD-LL37 and to extract information about the dynamics of its interactions with PC, and were compared to previous studies. Lastly, we were able to propose a unique mechanism for *f*CBD-LL37 and describe the role that adding *f*CBD has in determining mechanistic variations, and ultimately, determining the possible cytotoxic actions of *f*CBD-LL37. The results found in this project will further help the understanding of AMPs for future development in areas such as wound healing and replacing antibiotics.

Chapter 3: Materials and Methods

I. Materials

Synthetic LL37 (LLGDFFRKSKEKIGKEFKRIVQRIKDFLRRTES) was purchased from Anaspec, Inc. (Fremont, CA) at >95% purity. It was confirmed by high-performance liquid chromatography (HPLC).

The modified LL37 peptide with a fibronectin-derived CBD (fCBD-LL37) (LLGDFFRKSKEKIGKEFKRIVQRIKDFLRNLVPRTESDYKDDDDKCQDSERTFY) was synthesized by New England Peptide, Inc. (Gardner, MA) at >90% purity. This peptide was also confirmed by HPLC. A FLAG™ domain (DYKDDDDK) linker sequence was included between the LL37 and CBD sequences in each peptide to preserve flexibility, and as an epitope tag. The peptides were received at greater than 90% purity confirmed by high performance liquid chromatography. Stock solutions (0.67 mM) of each AMP were prepared according to manufacturer recommendations (LL37 in sterile PBS (pH 7.2) and cCBD- and fCBD-LL37 in sterile water (pH 3.5), each supplemented with 5 mM ethylenediaminetetraacetic acid (EDTA)) and stored at -20°C. Deionized water was taken from a MilliporeSigma Milli-Q Integral water purifier. Sodium chloride and tris(hydroxymethyl)aminomethane were purchased from Sigma-Aldrich. Peptide and lipid vesicle solutions were prepared in Tris–NaCl buffer (100 mM sodium chloride and 10 mM tris(hydroxymethyl)aminomethane at pH 7.8). Sodium hydroxide and hydrochloric acid were diluted from a stock solution to regulate the pH of the buffer. The QCM-D instrument used was purchased from Biolin Scientific along with QCM-D crystals that are coated in silicon dioxide (SiO_2)

II. Methodology

3.1 Tris-NaCl Buffer

A Tris-NaCL Buffer solution and SDS buffer solution were prepared by first measuring out 1.168g NaCl and 0.24 g Tris into a clean 250 mL beaker. Then, 200 mL of deionized (DI) water was added to the beaker. The beaker was then placed on a stir plate and the solution was stirred for approximately 5 minutes or until the mixture was dissolved. The pH meter was calibrated using the pH 7 and 10 solutions. After the NaCl and Tris dissolved, the pH of the solution was measured using the pH meter. The initial pH of the solution is usually around 8.5. The pH of the buffer solution was adjusted to pH 7.8 using HCl or NaOH to make the solution more acidic or basic.

3.2 Dilute Egg PC Solution

The initial concentration of egg PC solution is 2.5 mg/mL. The concentration of egg PC had to be diluted to 0.1 mg/mL in order to be ran through the quartz crystal microbalance with dissipation (QCM-D). To make a dilute lipid solution, the stock solution of lipids at 2.5 mg/mL PC egg solution were first vortexed. The test tube was cleaned with ethanol and a kimwipe. The concentrated lipid solution was diluted by first adding 0.24 mL of concentrated egg PC solution into a test tube containing 5.76 mL of Tris-NaCl buffer solution. Vortex the solution briefly prior to flowing through the QCM-D.

3.3 Freeze/Thaw Methodology

First, dry ice was obtained in a styrofoam container and broken into pieces for the test tube to be completely surrounded by ice. Then, the test tube containing the concentrated egg PC solution was placed at a slant in the container of dry ice between the crevices of the dry ice. The test tube was left in the container for about 15-20 minutes to allow the PC solution to freeze. After freezing, the test tube was placed into a water bath and the solids were monitored until a phase change from solid to liquid occured. The procedure was repeated for a total of 5 cycles. The freezing should take approximately 13-15 minutes, the thawing should take approximately 5-7 minutes and the vortexing should

be about 15 seconds for cycles 2-5. After following the above steps continue to sonication.

3.4 Sonication/Centrifugation

A 250 mL beaker was packed tightly with normal ice leaving very little extra space and the top of the cylinder was covered with foil. After completing the freeze/thaw cycles (part 3), the contents of the polyethylene tube were transferred into the open and parafilmed glass or plastic tube. The test tube was placed into the beaker filled with ice and taped to the aluminum foil to ensure that the test tube will not move. Finally, the test tube was sonicated for 30 minutes under the conditions listed in the table below.

Table 2: Sonicate test tube under these conditions

Sonication condition settings	
Mode:	Pulse mode
Amplitude setting:	60% Duty cycle
Frequency:	30 Hz
Time:	30 minutes 3 seconds on, 7 seconds off

After sonication the solution was then put in a centrifuge. Two new polyethylene test tubes were cleaned to place the liquid into a fresh test tube and add water to the other. More water was added to the test tube containing water to account for the weight because of the difference in density of the two (2) solutions. Both test tubes were placed in the centrifuge across from one another in order to balance the centrifuge. The centrifuge was operated at 15,000 RPM for 10 minutes. After 10 minutes both test tubes were removed. A micropipette was used to remove supementant (liquid) so as to not disturb the pellets and place into the other cleaned polyethylene test tube. The solution was dried with nitrogen or approximately 20 seconds and store the solution in the refrigerator at 4℃ for up to one (1)

month.

3.5 QCM-D Bilayer Formation Procedure

Silica-coated sensor crystals were placed into the QCM-D flow chambers and cleaned by flowing ethanol, deionized water and 2% sodium dodecyl sulfate (SDS) solution through all four (4) chambers at 0.35 mL/min. After cleaning, the sensors and chambers were dried with nitrogen gas. A Plasma Prep II, oxygen plasma cleaner, was used to etch the crystal's sensor surface before each experiment to remove the outer atomic layers of the crystal surface and make it more hydrophilic. Buffer was flowed over QCM-D sensors at 0.15 mL/min for approximately 15 min at 23℃ or until the frequency and dissipation response were stable. The lipid solution was flowed over the crystals for approximately 8 minutes to form a stable supported lipid bilayer (SLB). The crystals were rinsed with buffer to remove any unattached lipids. After establishing a baseline, peptide solution was added for 10 min, at which time the pump was stopped. QCM-D crystals were exposed to a stagnant peptide solution for 1 h, after which the peptide solution was replaced with a final buffer rinse at 0.15 mL/min until the frequency stabilized. After running the QCM-D to facilitate the vesicle rupture into a bilayer the sensor crystals were cleaned again by flowing ethanol, deionized water and 2% sodium dodecyl sulfate (SDS) solution through all four (4) chambers at 0.35 mL/min.

The bilayer formation was monitored by observing patterns in the QCM-D frequency and dissipation. After bilayer formation, the A complete bilayer could be characterized by a final Δf of -26 Hz and change in dissipation (ΔD) of $\sim 1 \times 10^{6}$ in the third harmonic. Then tris-NaCl buffer was flowed for 10 minutes, followed by the introduction of the *f*CBD peptide being flowed for 10 minutes. After peptide flow, the peptide was left to incubate for an hour. Followed by incubation there was a final flow or tris-NaCl buffer for 10 minutes. These procedures were repeated for all eight (8) concentrations.

3.7 Part 6: Data Analysis

As the experiment was being run by the QCM-D, the raw data was recorded in the QSoft software where we were able to monitor in real-time, the activity above the surface of the crystal. After completing the experiment, the data was then exported from QSoft to a different software called QTools, which allows us export the data onto an excel spreadsheet. The raw data was then organized on the excel spreadsheet and inputted into Sigmaplot. Sigmaplot was the software we used to create our real-time trace responses and bar graphs. We also ran statistical analyses (Anova, Tukey, and SNK) through this software.

Chapter 4: Results and Dicussions

At 0.01-0.25 µM concentration fCBD-LL37 does not interact significantly

Figure 3a:

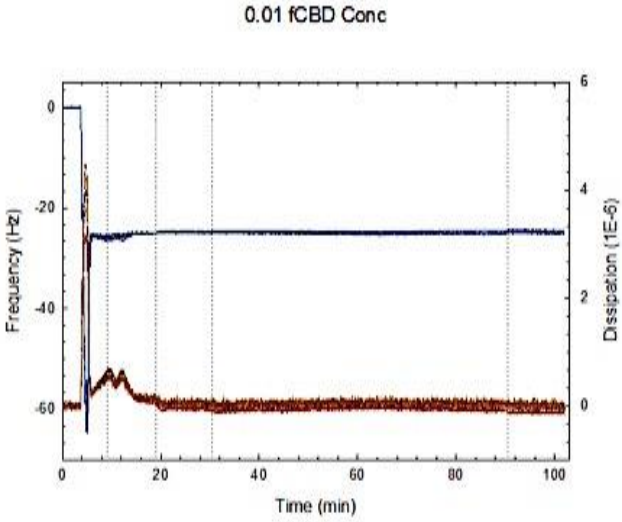

Figure 3b:

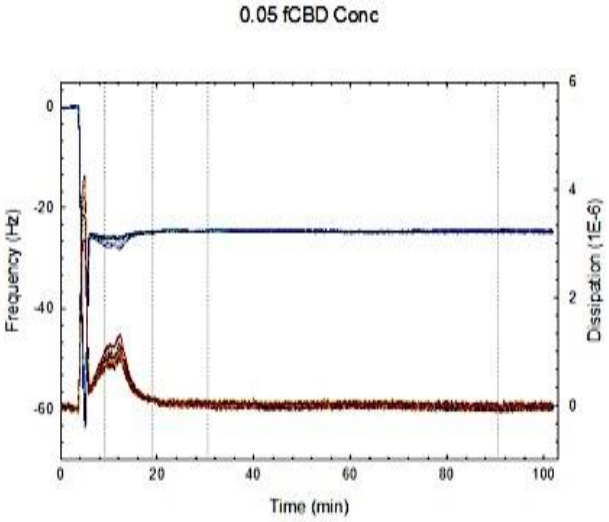

Figure 3c:

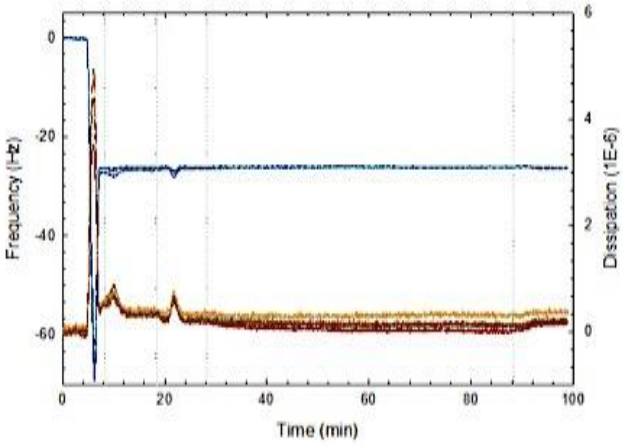

Figure 3d:

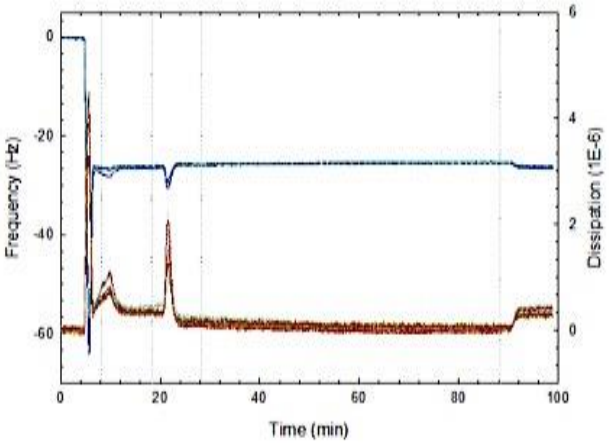

Figure 3: Figure 3a shows frequency (Δf) and dissipation (ΔD) vs time line plot graphed in SgimaPlot. This graph shows a replicated experiment using a QCM-D of 0.01 concentration fCBD-LL37. Figure 3b shows frequency (Δf) and dissipation (ΔD) vs time line plot graphed in SgimaPlot. This graph shows a replicated experiment using a QCM-D of 0.05 concentration fCBD-LL37. This graph shows one interaction pattern of two observed at 0.05 concentration. Figure 3c shows frequency (Δf) and dissipation (ΔD) vs time line plot graphed in SgimaPlot. This graph shows a replicated experiment using a QCM-D of 0.1 concentration fCBD-LL37. In this graph range of dispersion in the dissipation lines can be observed from ~0.0x10^6 to ~0.2x10^6. Figure 3d: Frequency (Δf) and dissipation (ΔD) vs time line plot graphed in SgimaPlot. This graph shows a replicated experiment using a QCM-D of 0.25 concentration fCBD-LL37. This graph shows the second interaction patterns observed at 0.25 concentration fCBD.

The lowest concentration studied, 0.01 μM, during bilayer formation, Δ*f* decreased to approximately -70 Hz when the vesicles adsorbed and showed an increase when the vesicles ruptured to form the bilayer (**Figure 3a**). The ΔD showed an increase to ~$6x10^6$ in response to the attachment of the water-filled vesicles. A complete bilayer could be characterized by a final Δ*f* of around -26 Hz and change in dissipation ΔD of approximately zero (0). The Δ*f* value remained constant throughout the experiment at approximately -26 Hz. After bilayer formation, ΔD increased to approximately $0.5x10^6$. The tris-NaCl buffer was introduced at the about 10 minutes and there was decreased in dissipation to $0.2x10^6$. Immediately after the decrease to $0.2x10^6$ the ΔD increased to $0.5x10^6$. The dissipation decreased at a steady rate to approximately zero (0) after peptide the peptide is introduced at 20 minutes and continues to remain at constant rate during peptide incubation and after the final buffer rinse at the last 10 minutes shown on the graph.

At 0.05 μM concentration *f*CBD-LL37 two different peptide interactions were observed

In **Figure 3b** after bilayer formation, tris-NaCl buffer was flowed at about 10 minutes and Δ*f* decreased to about -27 Hz. The frequency decreased at a steady rate to approximately -28 Hz after peptide was introduced at 20 minutes and continued to remain at a constant rate during peptide incubation and after the final buffer rinse at the last 10 minutes shown on the graph (**Figure 3b**). After the bilayer formation, ΔD increased drastically from ~$0.2x10^6$ to ~$1.8x10^6$. After this drastic increase, dissipation started to gradually decrease after 10 minutes to ~$0.1x10^6$. After 20 minutes, there was a small increase in ΔD to ~$0.5x10^6$ which then decreases to ~$0.2x10^6$. The ΔD value then increased to $1.0x10^6$ and stayed at a constant rate this the end of the experiment.

At 0.1 µM concentration fCBD-LL37 line graphs start to show more dispersion in the dissipation interaction patterns

Unlike 0.05 µM concentration *f*CBD, 0.1 *f*CBD µM showed one (1) interaction pattern (see **Figure 3c**). The concentration 0.1 µM *f*CBD, displayed reproducible interaction patterns throughout the various replicates. In **Figure 3c**, the graph shows similar interaction patterns to the graph in **Figure 3b.** After the introduction of peptide, Δf values decreased slightly from -26 Hz to -28 Hz. After 20 minutes, during peptide incubation Δf remained constant at -26 Hz till the end of the experiment. After tris-NaCl buffer was run at 10 minutes, ΔD increased from ~$0.1x10^6$ to ~$1.0x10^6$ followed by another decrease from ~$1.0x10^6$ to ~$0.1x10^6$. After the peptide was introduced, ΔD had a second (2) increase from ~$0.1x10^6$ to ~$0.8x10^6$. During peptide incubation, there was dispersion throughout the different overtones of ΔD until the final buffer run, where frequency values made a slight decline and dissipation values made an incline.

At 0.25 µM concentration fCBD-LL37 two different peptide interactions are shown

In **Figure 3d**, after bilayer formation, the buffer was flowed at about 10 minutes and Δf decreased to about -27 Hz. The frequency decreased at a constant rate until after the peptide was introduced after 20 minutes and there was a sudden decrease in Δf from -26 Hz to -31 Hz. After this sudden decrease, Δf increased to -25 Hz and remained constant during peptide incubation at until the final buffer rinse at 95 minutes. At the final buffer rinse Δf decreased at a steady rate to a final Δf value of -27 Hz. After the buffer was introduced, ΔD increased from ~$0.1x10^6$ to ~$1.2x10^6$ and then decreases to ~$0.2x10^6$. After peptide is introduced at 20 minutes, there is a drastic increase in dissipation from ~$0.2x10^6$ to ~$2.0x10^6$. Then, ΔD decreases down to zero (0) and remains constant at zero (0) during peptide incubation. The value of ΔD increases from zero (0) to ~$0.2x10^6$ after the final buffer rinse.

Trace patterns for concentrations 0.01-0.25 μM showed similar trace graph trends

When the bilayer was being formed the lipid vesicles first attached to the QCM-D sensor surface which added mass to the surface. The lipid vesicles then burst releasing the fluids within the vesicle forming a supported lipid bilayer (SLB). The frequency decreased when the vesicles were absorbed and then an increase in frequency was shown as soon as the vesicles ruptured to form the bilayer. The dissipation increased in response to the attachment of water-filled vesicles and after bilayer formation, dissipation decreased because the bilayer become more rigid than the vesicles. A complete bilayer could be characterized by a final Δf of ~26 Hz and change in dissipation (ΔD) of ~$1x10^{-6}$ in the third harmonic. However, our data was more focused on what happened after the lipid bilayer formation.

For concentrations 0.01-0.25 μM, when peptide was added and allowed to remain in contact with the bilayer, changes in frequency and dissipation were monitored continuously. The frequency responses at all overtones showed an initial decrease in frequency, and therefore an increase in mass, on the crystal as peptides attached to the bilayer. The dissipation responses at all overtones showed a decrease in dissipation suggests that the bilayer is becoming slightly more rigid.

Figure 4 shows all of the overall changes of frequency and dissipation bar graphs for the lower concentrations of *f*CBD-LL37. These graphs are based on a frequency and dissipation scale of -3 to 3 Hz and 1E-6, respectfully. The changes of frequency and dissipation are very low for these concentrations. It is evident from the graphs that there is a greater difference of the changes of frequency and dissipation along the 3rd overtone, therefore the 3rd overtone has the longest bar.

Bar graphs including errors for concentrations 0.01-0.25 µM

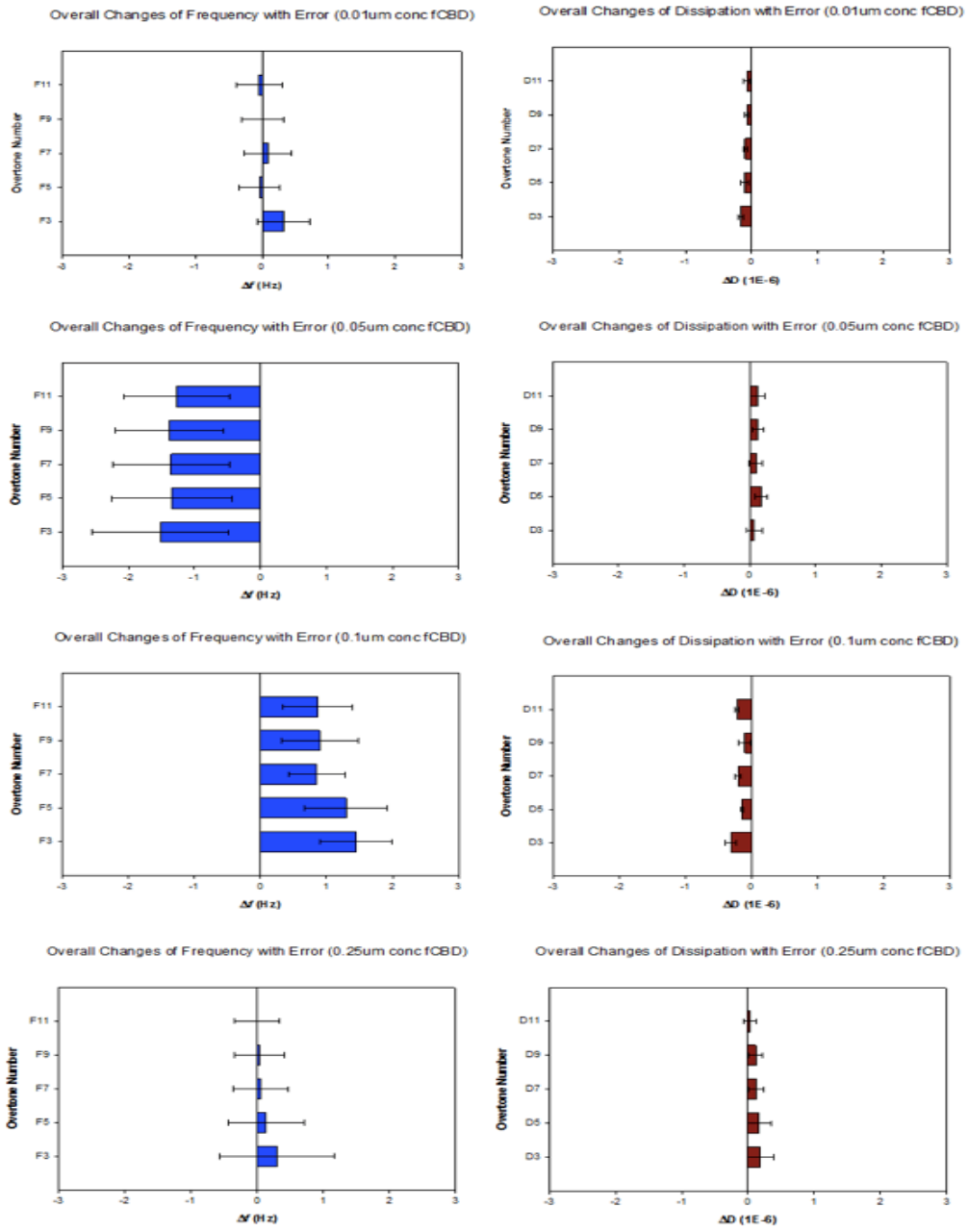

Figure 4: Bar graphs including error bars for fCBD-LL37 concentrations of 0.01-0.25 µM

For these concentrations, we performed a one-way ANOVA statistical analysis. This analyses showed that the variation in the overall Δ*f* and ΔD were too insignificant. This insignificance means that there is not a lot of interaction occurring at the bilayer so there is no need for a further statistical analysis using the Tukey or SNK method.

At 0.5 µM concentration fCBD-LL37 the graphs start showing a more noticeable decrease in Δf values

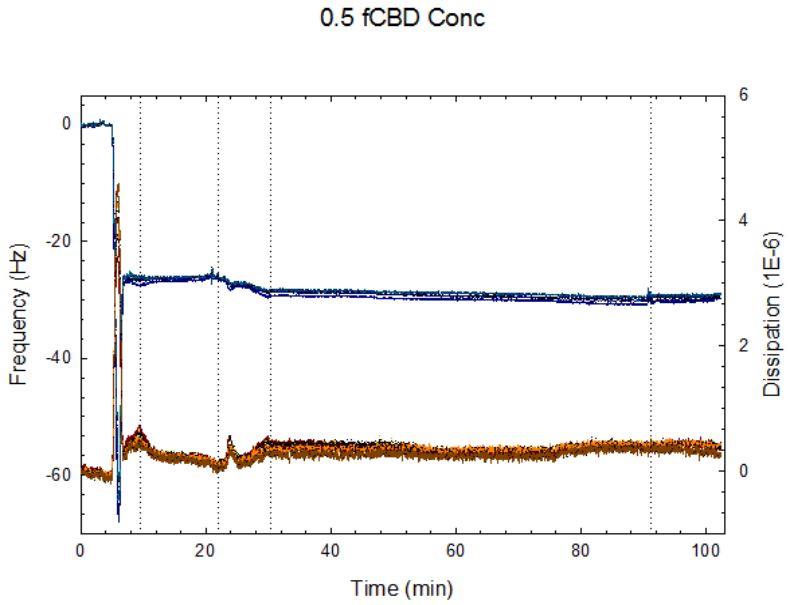

Figure 5: Frequency (Δf) and dissipation (ΔD) vs time line plot graphed in SgimaPlot. This graph shows a replicated experiment using a QCM-D of 0.5 concentration fCBD-LL37. In this graph range of dispersion in the dissipation lines can be observed from ~0 to ~0.5 x10^{6}

The concentration 0.5 µM *f*CBD, displayed reproducible interaction patterns throughout the various replicates. After bilayer formation, Δ*f* remained constant around -26 Hz until the peptide was introduced and there was a decrease from -26 Hz to -30 Hz. During peptide incubation Δ*f* remained constant at -30 Hz until the final buffer rinse where there was a very small increase to -29 Hz. While Δ*f* was decreasing, the ΔD values increase

with dispersion in the overtones of Δ*f* and ΔD. After the buffer was introduced, ΔD values increase from ~0.1x10^6 to ~0.5x10^6 and decreased from ~0.5x10^6 to zero (0) at about 20 minutes. After the peptide was introduced, ΔD increased from zero (0) to about 0.4x10^6. During peptide incubation ΔD increased from ~zero (0) to ~0.1x10^6 and remained constant until the end of the experiment.

An increase in dissipation indicates that the bilayer is becoming more rigid. However, the changes of frequency didn't decrease which suggests that mass was not added onto the surface of the bilayer. This shows that there are minimal amounts of peptide attaching to the surface of the bilayer.

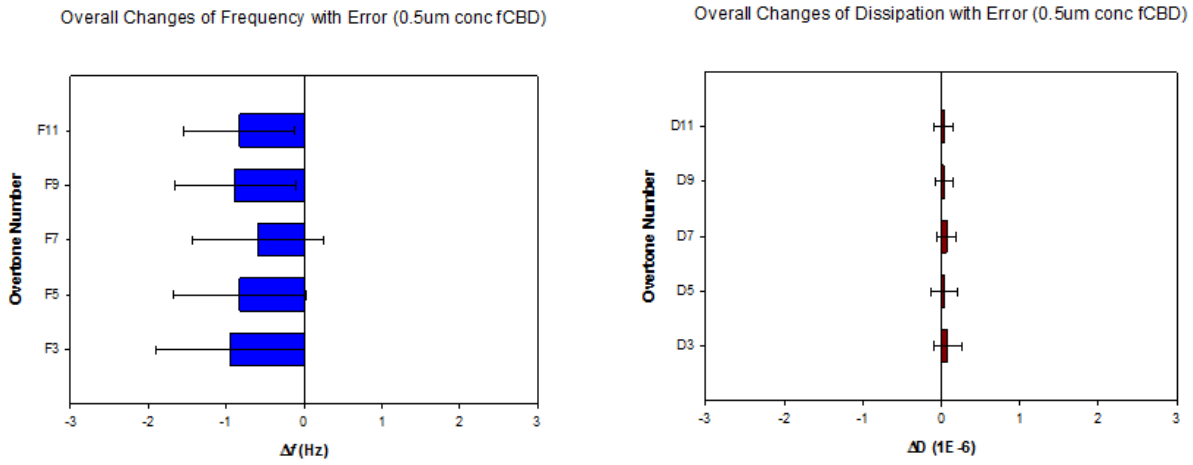

Figure 6: Bar graphs including error bars for fCBD-LL37 concentrations of 0.5 μM

The figure above represents the bar graph for 0.5 μM concentration peptides. We are able to see that as frequency decreases, dissipation barely increases. From the trace responses, we were not able to fully tell if the frequency values were decreasing or increasing, but from the bar graphs, it is clear that the dissipation values increase slightly. Like stated earlier, this could indicate that there is only some attachment of peptide onto the surface of the bilayer.

At 1.0 µM concentration fCBD two (2) interaction patterns were observed with different dispersions throughout the overtones

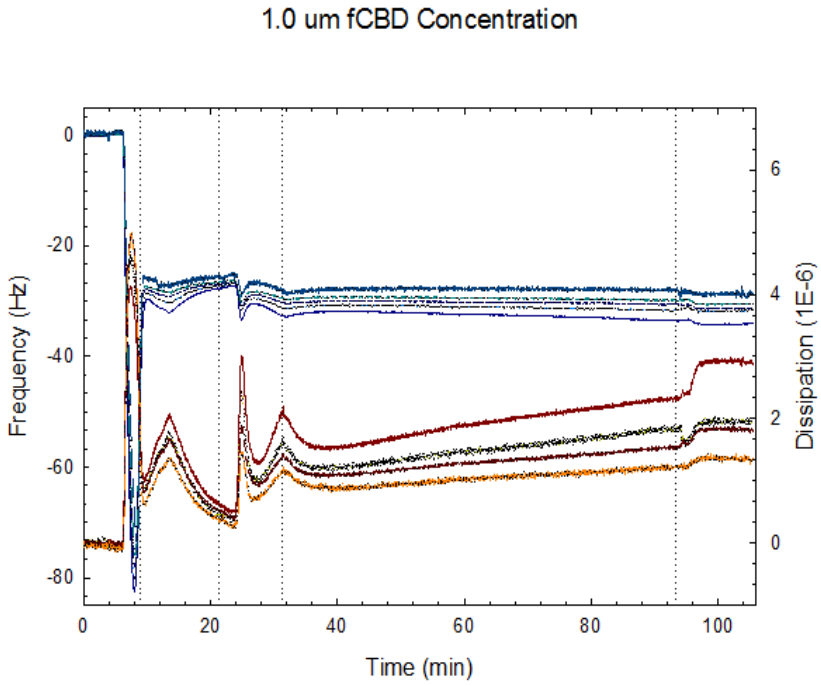

Figure 7: Frequency (Δf) and dissipation (ΔD) vs time line plot graphed in SgimaPlot. This graph shows a replicated experiment using a QCM-D of 1.0uM concentration fCBD-LL37. In this graph range of dispersion in the dissipation lines can be observed from ~1.2x10^6 to ~3 x10^6 and frequency lines can be observed from ~-37 Hz to ~-27 Hz.

In **Figure 7,** after the bilayer is formed, there is decrease in Δ*f* from -26 Hz to -38Hz. The value of Δ*f* remains relatively constant at -32 Hz until after the peptide is introduced where Δ*f* shows a decrease from -26 Hz to -38 Hz. The Δ*f* values in the overtones start to disperse more creating more distance between the overtones, ranging from -26 Hz to -38 Hz. After the peptide was introduced, ΔD increased from ~0.1x10^6 to ~3.1x10^6. During the incubation period, the 3rd harmonic increased to around 1.8x10^6 while the remaining harmonics remained at around 1x10^6. After the final buffer rinse, there

is a slight decrease of frequency to around -36 Hz and an increase of dissipation of the 3rd harmonic to about $2.1x10^6$ and the remaining harmonics to about $1.8x10^6$.

Starting from this concentration, we were able to notice more dispersion of the overtones in the trace responses. It was more evident that as dissipation increased, frequency decreased which indicates that mass is being adsorbed onto the surface of the bilayer. The separation of the 3rd overtone from the other overtones indicate that there is more activity along the surface of the bilayer only which indicates that the peptides are just attaching to the surface and not penetrating through the bilayer.

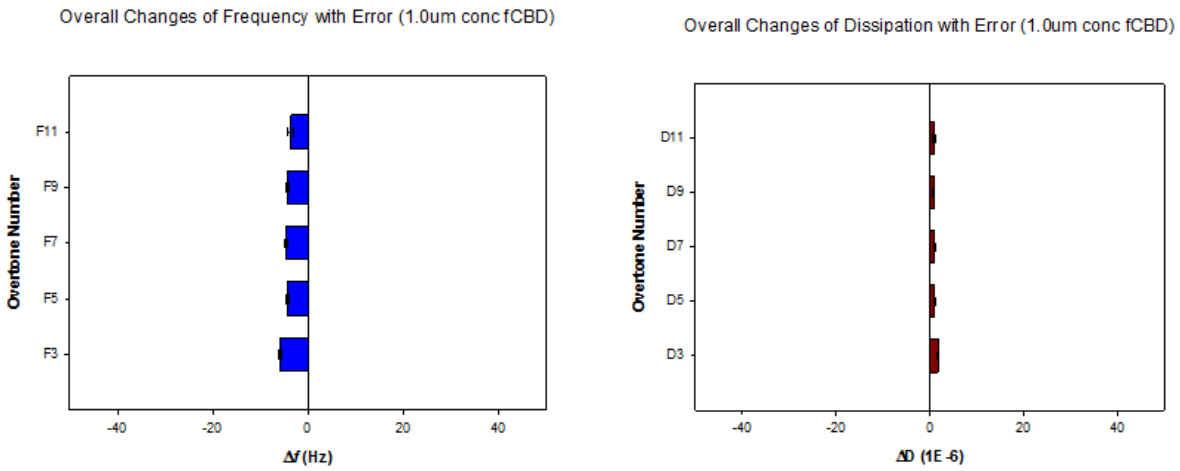

Figure 8: Bar graphs including error bars for fCBD-LL37 concentrations of 1.0 µM

Similar to the bar graphs for the 0.5 µM concentration of *f*CBD-LL37, the general trend of the changes of frequency and dissipation along the bilayer is the same. However, now the scale in which we measure our data is much higher at -50 to 50 Hz and 1E-6, respectively. This suggests that along the surface of the bilayer, there is more evidence of antimicrobial activity.

Higher concentrations of 5.0 µM and 10.0 µM concentration fCBD show the greatest range of dispersion in Δ*f* and ΔD

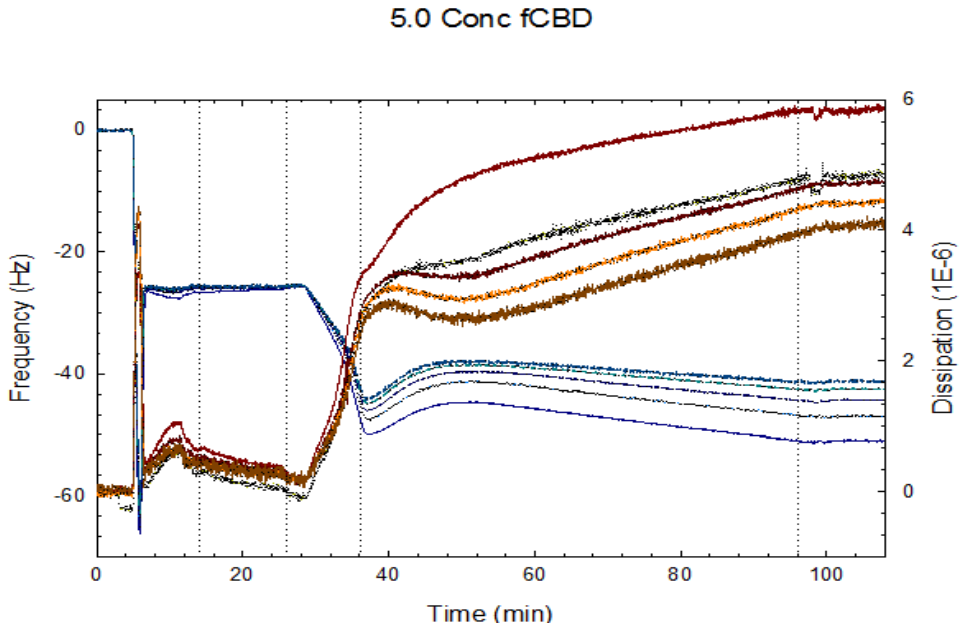

Figure 9: Frequency (Δf) and dissipation (ΔD) vs time line plot graphed in SgimaPlot. This graph shows a replicated experiment using a QCM-D of 5.0uM concentration fCBD-LL37. In this graph range of dispersion in the dissipation lines can be observed from ~0.9x10^6 to ~1.8 x10^6 and frequency can be observed from ~-21 Hz and 1Hz.

Experiments carried out using peptide concentrations 5.0 µM (**Figure 9)** and 10.0 µM concentration showed reproducible graphs for all six (6) replicates of each concentration, see Appendix B. After bilayer is formed Δ*f* remains constant at -26 Hz until the peptide is introduced at 25 minutes and Δ*f* values decrease from -26 Hz to -50 Hz. During peptide incubation, Δ*f* values slightly increase from -50 Hz to -40 Hz and there is dispersion throughout all the Δ*f* overtones ranging from -40 Hz in the 3rd overtone to -50 in the 11th overtone. After bilayer formation, the value of ΔD increased from zero (0) to ~1.3x10^6 and when buffer was introduced ΔD decreased from ~1.3x10^6 to ~0.1x10^6. At 25 minutes when peptide is flow through the QCM-D the frequency drastically decreased to approximately -50 Hz, while the dissipation increased to ~3.5x10^6. During incubation, the dissipation overtones started to disperse more having a greater distance between the

different overtones, ranging from around $4.0x10^6$ in overtone 11 to $6.0\ x10^6$ in overtone 3.

At the concentration of 5.0 µM *f*CBD there is even greater dispersion throughout the frequency and dissipation trace responses than at concentration 1.0 µM *f*CBD. Using a peptide of 5.0 µM there is a greater decrease in frequency which indicates that there is an even greater adsorption of mass to the surface of the bilayer indicating that the bilayer is becoming more rigid by the addition of mass and increase in dissipation. Similarly, to 1.0 µM the separation of the 3rd overtone from the other overtones indicate that there is more activity along the surface of the bilayer only which indicates that the peptides are just attaching to the surface and not penetrating through the bilayer.

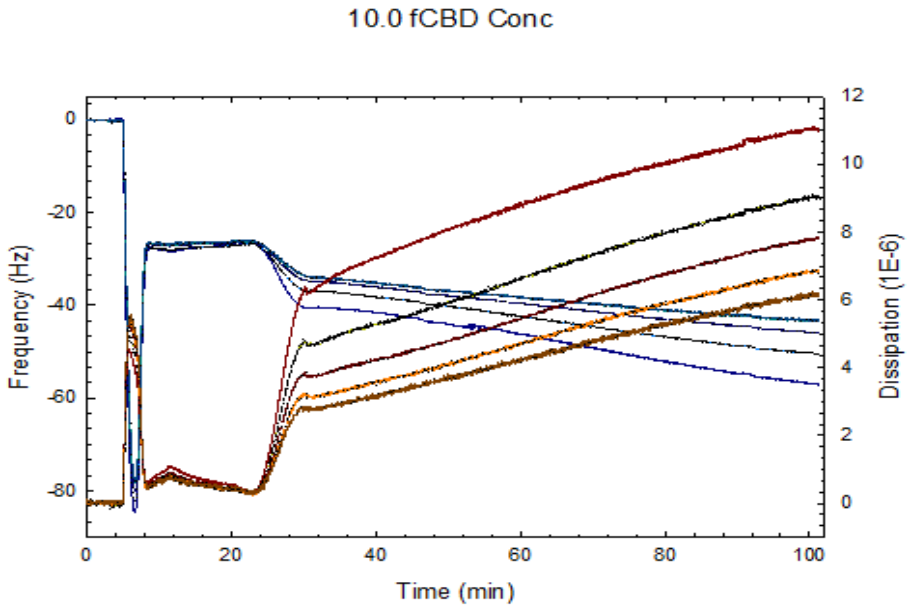

Figure 10: Frequency (Δf) and dissipation (ΔD) vs time line plot graphed in SgimaPlot. This graph shows a replicated experiment using a QCM-D of 5.0uM concentration fCBD-LL37. In this graph range of dispersion in the dissipation lines can be observed from ~0.9x10^6 to ~1.8 x10^6 and frequency can be observed from ~-21 Hz and 1Hz.

Similar to the 5.0µM *f*CBD, experiments carried out using 10.0 µM showed reproducible end values of Δf and ΔD. After bilayer is formed Δ*f* remains constant at -26 Hz until the peptide is introduced at 25 minutes and Δ*f* values decrease from -26 Hz to -46 Hz. During peptide incubation, Δ*f* values decrease from -46 Hz to -60 Hz and there is dispersion throughout all the Δ*f* overtones ranging from -36 Hz in the 3rd overtone to -46

Hz in the 11th overtone. After bilayer formation, the value of ΔD increased from zero (0) to ~0.1x10^6 and when buffer was introduced ΔD decreased from ~0.1x10^6 to zero (0). At 25 minutes when peptide is flow through the QCM-D the ΔD drastically increased to ~6.0x10^6. During peptide introduction (**Figure 10**), frequency decreased and dissipation values increased from ~3.0x10^6 to ~6.0x10^6 until the lines overlapped during incubation. Dissipation values ranged from about ~6.0x10^6 to ~11.0x10^6 and frequency values ranged from about -44 Hz to -59 H.

For this concentration, the frequency and dissipation changes cross one another completely. This suggests that the peptide is penetrating through the bilayer instead of just attaching to the surface. For this concentration, there is separation along all of the overtones which means that there is antimicrobial activity along the overtones, therefore validating that the peptide is penetrating through the bilayer.

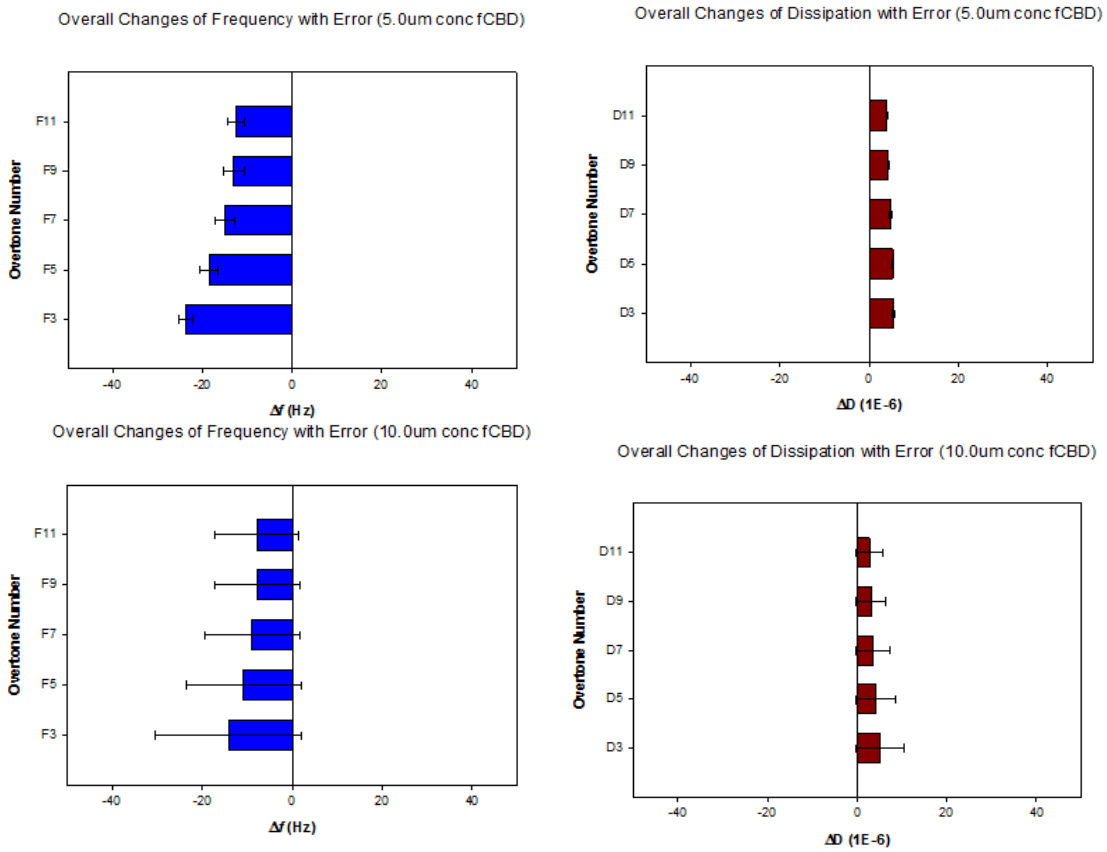

Figure 11:Bar graphs including error bars for fCBD-LL37 concentrations of 5.0 and 10.0 μM, as labeled

Similar to all other bar graphs described previously, as the overall changes of frequency increase, dissipation decreases. The 3rd overtone shows a greater difference in all cases indicating that there is increased activity along the 3rd overtone, which is the surface of the bilayer.

Chapter 5: Conclusions and Recommendations

In order to develop a broad-spectrum chronic wound collagen dressing based on antimicrobial peptides (AMPs) or a bacteria resistant antibiotic based on AMPs, several obstacles have to be overcome. Due to the AMPs' broad spectrum antimicrobial activity and anti-biofilm properties, they pose as an excellent alternative for current treatments for chronic wound infections and antibiotic resistant bacteria. The major reasons why AMPs have not been used for clinical applications is because the production cost is too high, costing $300-$500 per gram, and their mechanisms of action which is how they would interact in the body is still not understood well enough (Bray 2003; Vlieghe et al. 2010). These experiments carried out allowed us to observe how adding *f*CBD affected LL37 bioactivity, provided a foundation for future research, and will eventually aid in the development of biopolymer-tethered AMPs for wound healing applications.

In this study, the goal was to determine the action mechanism of one of these CBD peptides, *f*CBD-LL37 with a CBD derived from fibronectin, against zwitterionic phosphatidylcholine (PC) lipid bilayers. using a quartz crystal microbalance with dissipation (QCM-D). The QCM-D has a nondestructive flow making it able to collect data in realtime. We chose to study *f*CBD-LL37 because from prior research, it is found that fCBD is less cytotoxic than LL37 and *c*CBD-LL37 and preserves its antimicrobial activity (Lozeau et al, 2016). After carrying out experiments for eight (8) different concentrations with six (6) different replicates we observed some general trends in the data we collected (**Appendix B**). For all concentrations and replicates we took into consideration the time dependency of the experiment, peptide concentration and the lipid solution that was used. In general, it was shown that overall changes in dissipation (ΔD) and frequency (Δf) increase with higher concentrations of *f*CBD.This addition of mass can easily be seen in these higher concentrations due to the overtones being more spread out. For all concentrations of *f*CBD the outcomes of ΔD and Δf are relatively similar but they may

approach the mechanism via different pathways.

General trends from the trace responses and Anova analyses show that for concentrations of *f*-CBD lower than 0.5um, the P value, which indicates the degree of significance of activity along the bilayer, is less than 0.05. Thus, deeming the data insignificant for further Tukey and SNK analysis. However, for concentrations of *f*-CBD from 0.5um-10.0um, produced P values lower than 0.05. For each of these higher concentrations, a Tukey and SNK analysis were completed. The results of these analyses showed that there is a great difference of depth between the 3rd and 5th overtones versus the 11th overtone, suggesting more activity along the surface of the bilayer. This indicates that the peptides are being attached to the surface of the bilayer but not completely penetrating the bilayer.

The replicates of each concentration showed similar trace patterns within each concentration. For the concentrations 0.05 µM, 0.25 µM and 1.0 µM we observed two (2) different trace patterns which could suggest that there are two (2) different mechanisms of action present. From previous research, we know that LL37 usually displays either the non-pore carpet model or the detergent-like carper model Porcelli *et al.*, 2008). The research showed two (2) different trace patterns which could indicate that *f*CBD, like LL37, might display either the non-pore carpet model, the detergent-like carper model or both mechanisms. Due to the inconsistencies of the appearances of the peaks along the experiments, we also believe that it may not be a different mechanism, but rather some human error or software error. We recommend that further analysis be done by modeling the peptide-lipid interaction to monitor how the peptide is attaching the lipid surface in order to determine the exact mechanisms.

This is an important and interesting research topic and we recommend that more people continue looking into *f*CBD-LL37 as a possible AMP for clinical use. For future

analysis more experimental replicates of each concentration need to be done keeping the variables more constant. The QCM-D is a highly sensitive piece of equipment that is affect by the slightest movements by user handling and different solutions being flown through. We also recommend consistency in the preparation of the peptide and lipid solutions because differences in those also affect the graphs.

The long term goal of this research is the determine an improved method of treatment for chronic wound infections and functional tissue repair. The research required to fully improve treatments is still yet insufficient and more analyses and modeling is needed to gain a better understanding of the specific mechanisms. A better understanding of the AMP structure function relationship in the tethered state is vital for the success of the efforts to develop a more efficient treatment method. We believe that determining how to use AMPs for clinical treatment will solve various health issues which would fix the problem with a permanent solution rather than putting a band aid on it and only fixing it temporarily. The achievement of this research will be beneficial for the improvement of patient health.

References

· Bagheri, M.; Beyermann, M.; and M. Dathe. Immobilization Reduces the Activity of Surface-Bound Cationic Antimicrobial Peptides with No influence upon the Activity Spectrum. *Antimicrobial Agents and Chemotherapy*, **2008**, *53(3)*, 1132-41.

· Bahar, Ali Adem, and Dacheng Ren. "Antimicrobial Peptides." *Pharmaceuticals*. MDPI, 6 Dec. 2013. Web. 23 Jan. 2017.

· Blair, Jessica M.A., Mark A. Webber, Alison J. Baylay, David O. Ogbolu, and Laura J.V. Piddock. "Molecular mechanisms of antibiotic resistance." *Nature.com*. Macmillan Publishers, 1 Dec. 2014. Web. 23 Jan. 2017.

· Christina M Bailey, Elaheh Kamaloo, Kellie L Waterman, Kathleen F Wang, Ramanathan Nagarajan, Terri A Camesano. Size dependence of gold nanoparticle interactions with a supported lipid bilayer: A QCM-D study**,***Biophysical chemistry*, **2015**, *203***,** 51-61.

· "Chronic Wounds." *Chronic Wounds: Overview, The Biology of Wound Healing, Common Chronic Wounds*. N.p., n.d. Web. 23 Jan. 2017.

· Diamond, Gill, Nicholas Beckloff, Aaron Weinberg, and Kevin O. Kisich. "The Roles of Antimicrobial Peptides in Innate Host Defense." *Current pharmaceutical design*. U.S. National Library of Medicine, 24 Sept. 2009. Web. 23 Jan. 2017.

· Duplantier, A.J.; and M.L. van Hoek. The Human Cathelicidin Antimicrobial Peptide LL-37 as a Potential Treatment for Polymicrobial Infected Wounds. *Fronteirs in Immunology*, **2013**, *4(143)*, 1-14.

· Lawall. "Treatment of chronic wounds." *Treatment of chronic wounds: Vasa: Vol 41, No 6*. Hogrefe, 7 Jan. 2013. Web. 23 Jan. 2017.

· Marshall, ByHelen. "Treatments for bacterial infections (antibiotics)." *Treatments for bacterial infections*. Netdoctor, 02 Nov. 2015. Web. 23 Jan. 2017.

· Onaizi, S.A. and S.S.J. Leong. Tethering Antimicrobial Peptides: Current Status and Potential Challenges. *Biotechnology Advances*, **2011**, *29(1)*, 67-74.

· Sorensen, O.E.; *et. al*. Human Cathelicidin, hCAP-18, is Processed to the Antimicrobial Peptide LL-37 by Extracellular Cleavage with Proteinase 3. *Blood*, **2001**, *97*, 3951-9.

· Wang, K.F.; Nagarajan, R.; and T.A. Camesano. Antimicrobial Peptide Alamethicin Insertion into Lipid Bilayer: A QCM-D Exploration. *Colloids and Surfaces B: Biointerfaces*, **2014**, *116(1)*, 472-81.

· Wang, K.F.; Nagarajan, R.; C.M. Mello; and T.A. Camesano. Characterization of Supported Lipid Bilayer Disruption by Chrysophsin-3 Using QCM-D. *The Journal of*

Physical Chemistry B, **2011**, *115(51)*, 15228-35.

· Wang, K.F.; Nagarajan, R.; and T.A. Camesano. Differentiating Antimicrobial Peptides Interacting with Lipid Bilayer: Molecular Signatures Derived from Quartz Crystal Microbalance with Dissipation Monitoring. *Biophysical Chemistry*, **2015**, *196*, 53-67.

· Why are bacteria becoming resistant to antibiotics? *RxList*. RxList, n.d. Web. 23 Jan. 2017.

Appendix A: Examples of Antibiotics Currently Being Used and Their Functions

Table 2: Examples of antibiotics currently being used and their functions

Type of Antibiotic	Function of Antibiotic	Examples of Antibiotic
Aminoglycoside Antibiotics	Aminoglycoside antibiotics work by inhibiting bacterial protein synthesis. They are not well absorbed when given by mouth so are often given by injection, but may also be given as drops for some ear or eye infections. These antibiotics are only used when other antibiotics are not suitable or have not been effective, because they can sometimes cause problems with the kidneys or with hearing.	• Amikin (amikacin) • Cidomycin injection (gentamicin) • Genticin injection (gentamicin) • Tobi nebuliser solution (tobramycin) • Tobramycin injection • Nivemycin (neomycin)
Cephalosporin Antibiotics	Cephalosporins are a group of broad-spectrum antibiotics that are commonly used to treat infections caused by a wide variety of bacteria, including more serious infections such as septicaemia, pneumonia, meningitis, biliary-tract infections, peritonitis, and urinary-tract infections.	• Cefadroxil • Cefotaxime • Ceporex (cefalexin) • Distaclor (cefaclor) • Distaclor MR (cefaclor) • Fortum (ceftazidime) • Keflex (cefalexin) • Keftid (cefaclor) • Nicef (cefradine) • Orelox (cefpodoxime) • Rocephin (ceftriaxone) • Suprax (cefixime)

		• Zinacef (cefuroxime) • Zinnat (cefuroxime)
Macrolide Antibiotics	Macrolide antibiotics have an antibacterial spectrum that is similar, but not identical, to that of penicillin, so are often used for people with a penicillin allergy or to treat penicillin-resistant strains of bacteria. Macrolide antibiotics are particular useful for treating lung and chest infections. They are also used for skin infections and some sexually transmitted infections.	• Clamelle (azithromycin) • Erythromycin • Ketek (telithromycin) • Klaricid (clarithromycin) • Klaricid XL (clarithromycin) • Tiloryth (erythromycin) • Zithromax (azithromycin)
Penicillin Antibiotics	Penicillin antibiotics are the most widely used groups of antibiotics. They are mainly broad-spectrum antibiotics that can be used for a wide variety of infections, such as respiratory tract infections, skin infections and urinary tract infections. Flucloxacillin is reserved for treating bacteria that are resistant to other penicillins.	• Amoxicillin (eg Amoxil) • Co-amoxiclav (eg Augmentin) • Co-fluampicil • Crystapen (benzylpenicillin) • Flucloxacillin (eg Floxapen) • Magnapen (co-fluampicil) • Penbritin (ampicillin) • Penicillin V (phenoxymethylpenicillin) • Selexid (pivmecillinam) • Tazocin (piperacillin, tazobactam) • Timentin (ticarcillin)

Quinolone Antibiotics	These are broad-spectrum antibiotics that can be used to treat a wide range of infections, particularly urinary tract and respiratory infections.	• Avelox (moxifloxacin) • Ciproxin (ciprofloxacin) • Nalidixic acid • Tarivid (ofloxacin) • Tavanic (levofloxacin) • Utinor (norfloxacin)
Sulphonamide Antibiotics	The use of sulphonamides has decreased due to an increase in bacterial resistance and the development of other antibiotics that are more effective.	• Septrin (co-trimoxazole) • Sulfadiazine
Tetracycline Antibiotics	Tetracycline antibiotics such as minocycline and oxytetracycline are commonly used to treat moderate to severe acne and rosacea, but can also be used to treat a wide range of other bacterial infections, including respiratory and genital infections.	• Aknemin (minocycline) • Demeclocycline • Doxycycline (Vibramycin-D, Vibrox) • Oxytetracycline • Tetracycline tablets • Lymecycline (eg Tetralysal)
Other antibiotics	There are several other antibiotics that don't fit into the groups above. These are used for more specific types of infections.	• Azactam (aztreonam) • Chloramphenicol capsules • Clofazimine • Colomycin injection (colistin) • Cubicin (daptomycin) • Dalacin C capsules (clindamycin) • Dificlir (fidaxomicin) • Fasigyn (tinidazole) • Flagyl suppositories (metronidazole)

		• Flagyl tablets (metronidazole) • Fucidin suspension (fusidic acid) • Fucidin tablets (sodium fusidate) • Hiprex (methenamine) • Kemicetine (chloramphenicol) • Meronem (meropenem)

Appendix B: Frequency vs Dissipation Graphs

0.01 µM concentration fCBD

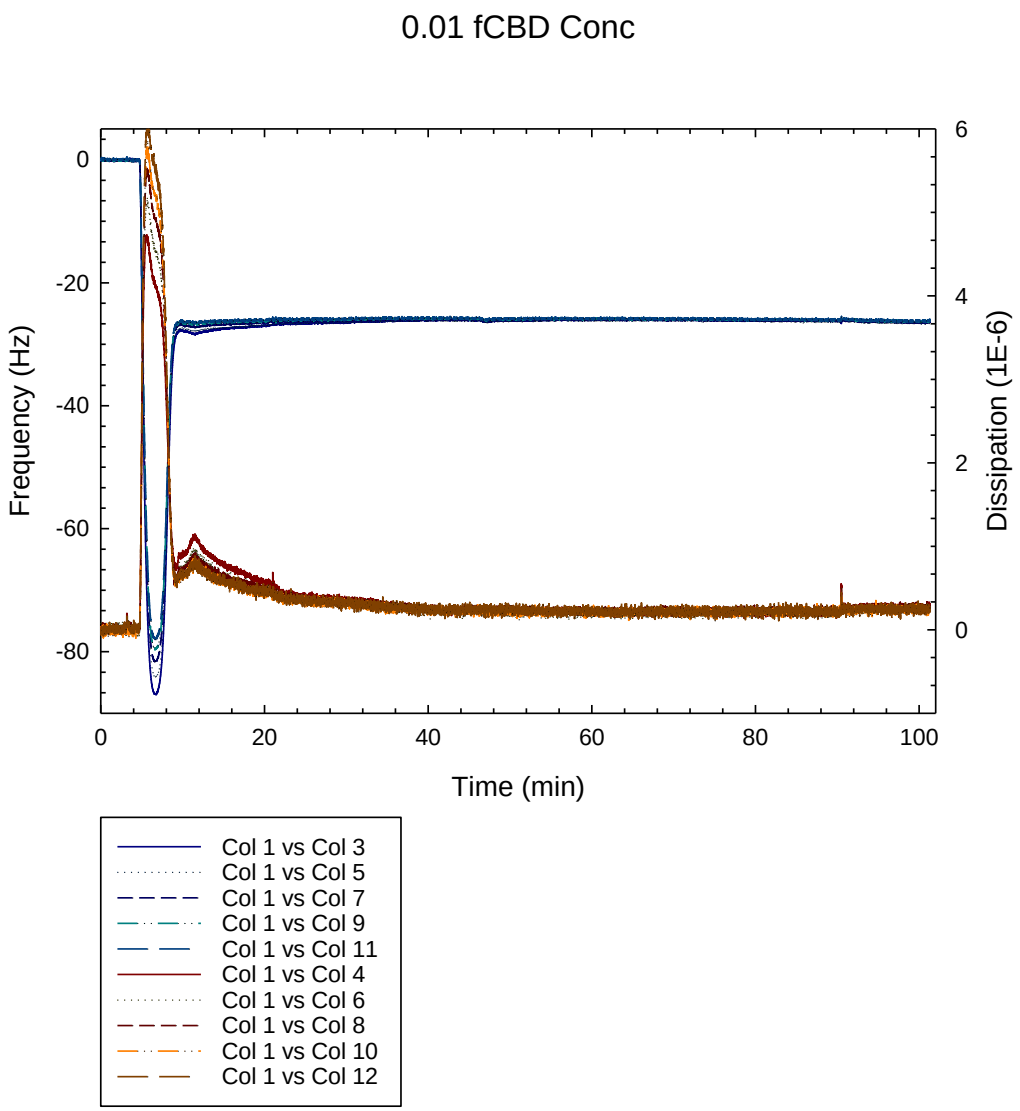

0.01 µM concentration fCBD

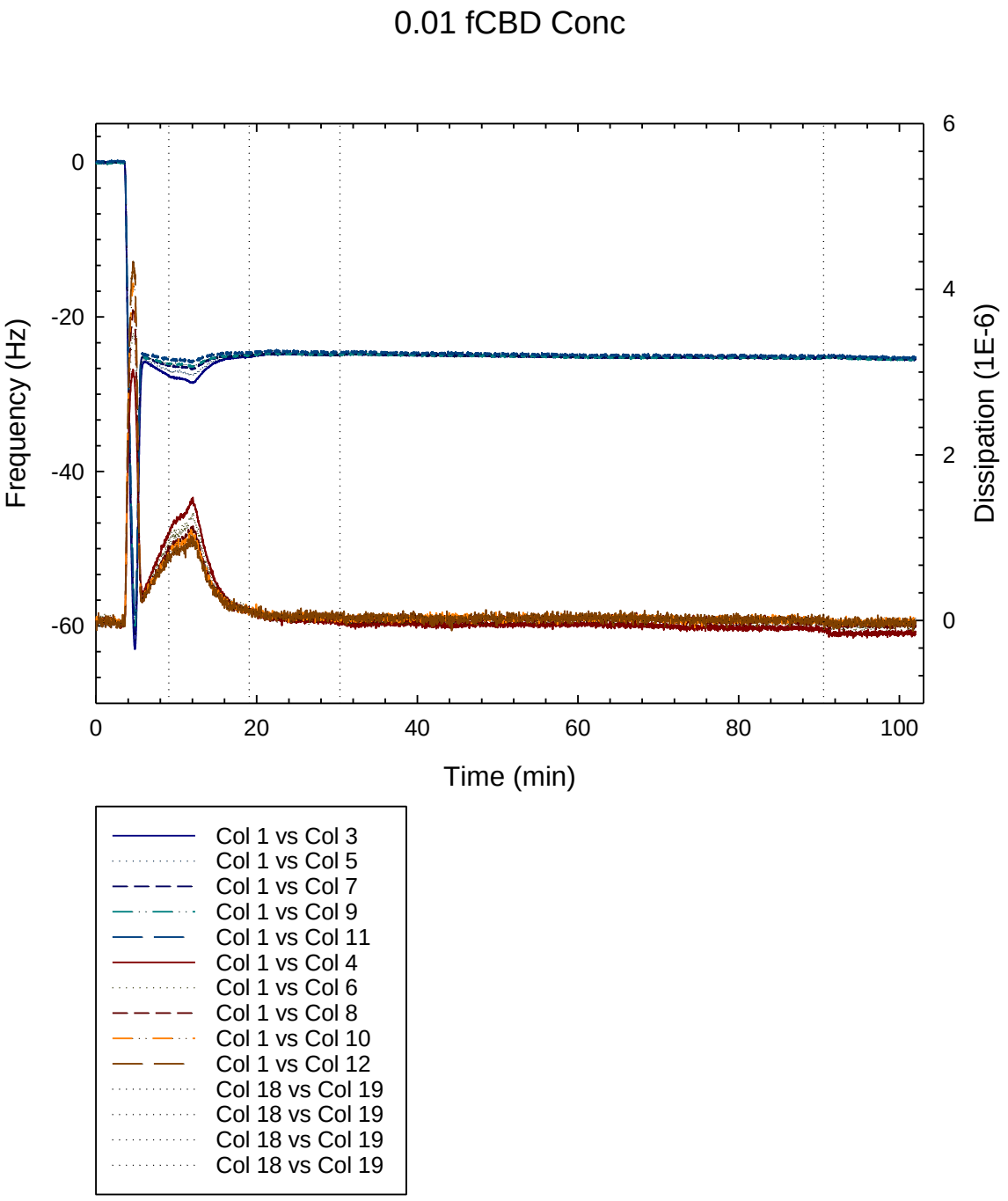

0.01 µM concentration fCBD

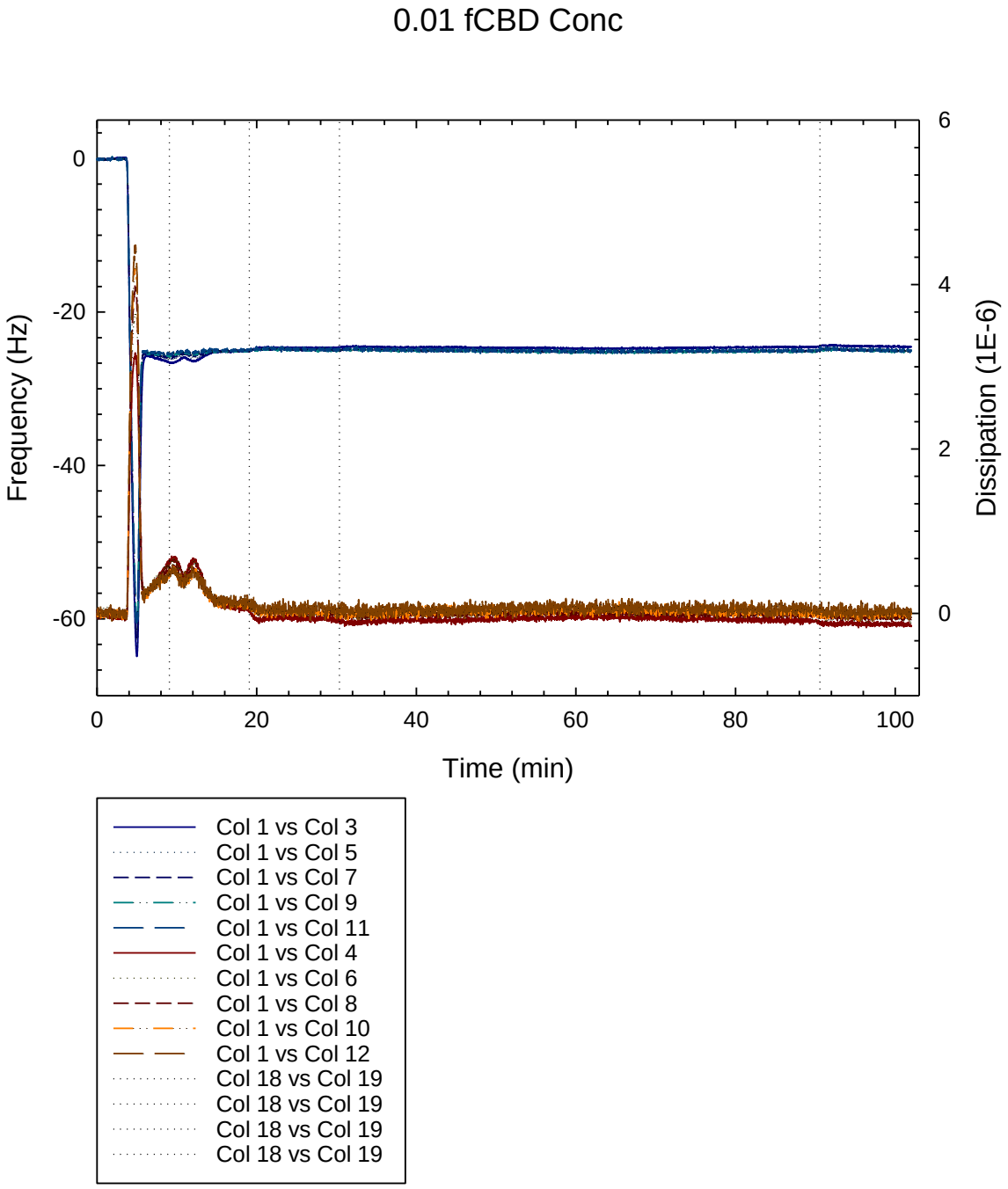

0.01 µM concentration fCBD

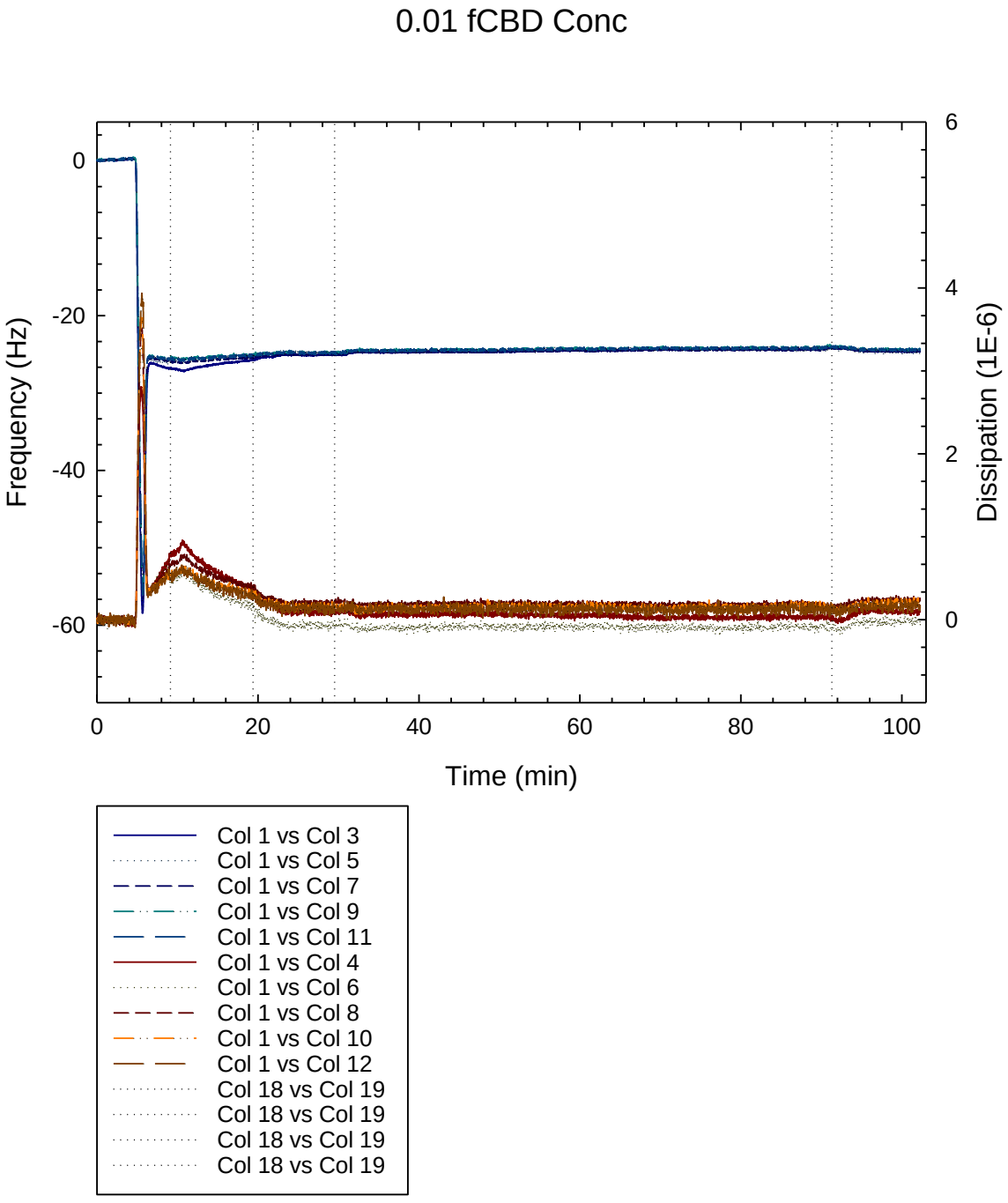

0.01 µM concentration fCBD

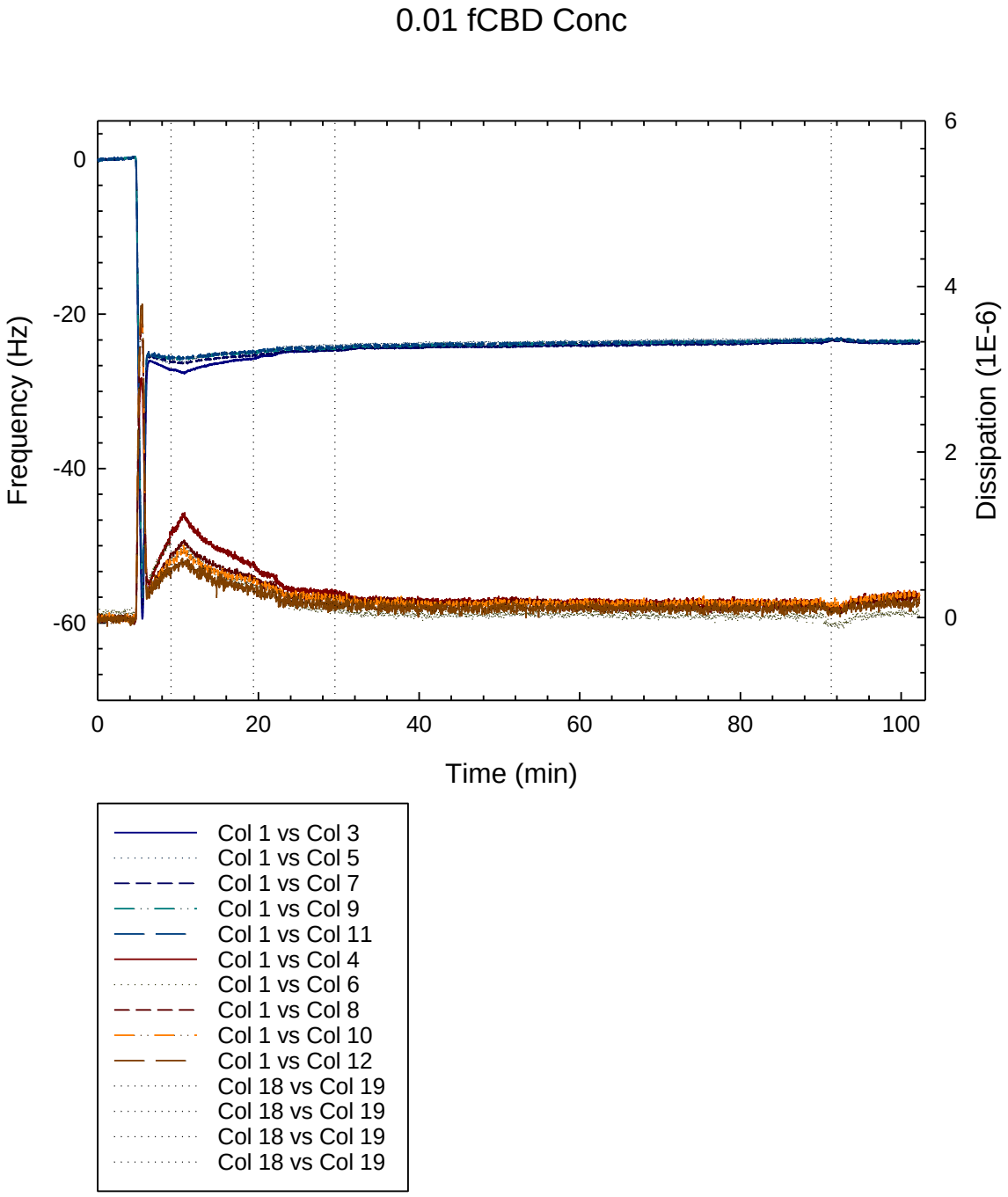

0.05 µM concentration fCBD

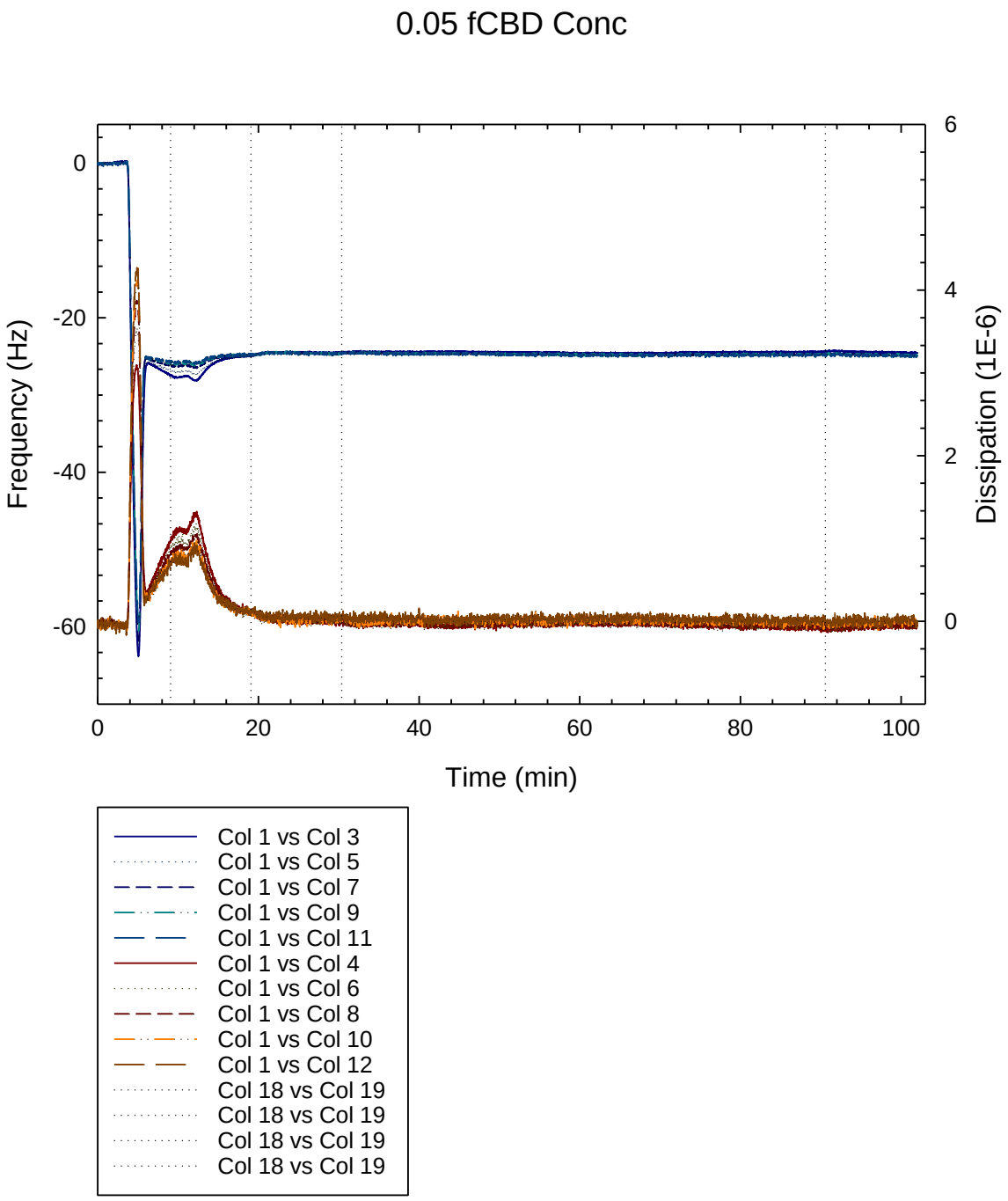

0.05 µM concentration fCBD

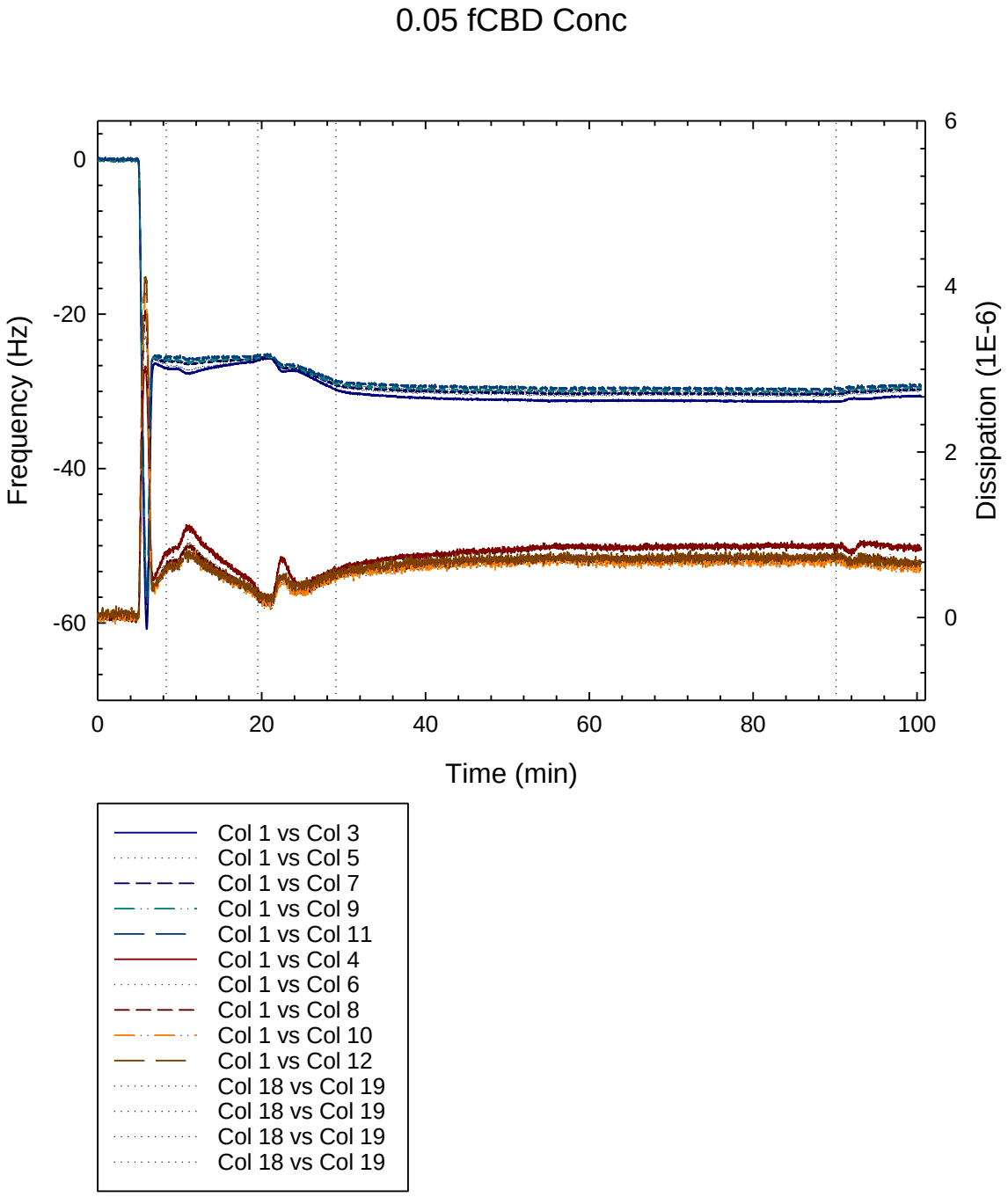

0.05 µM concentration fCBD

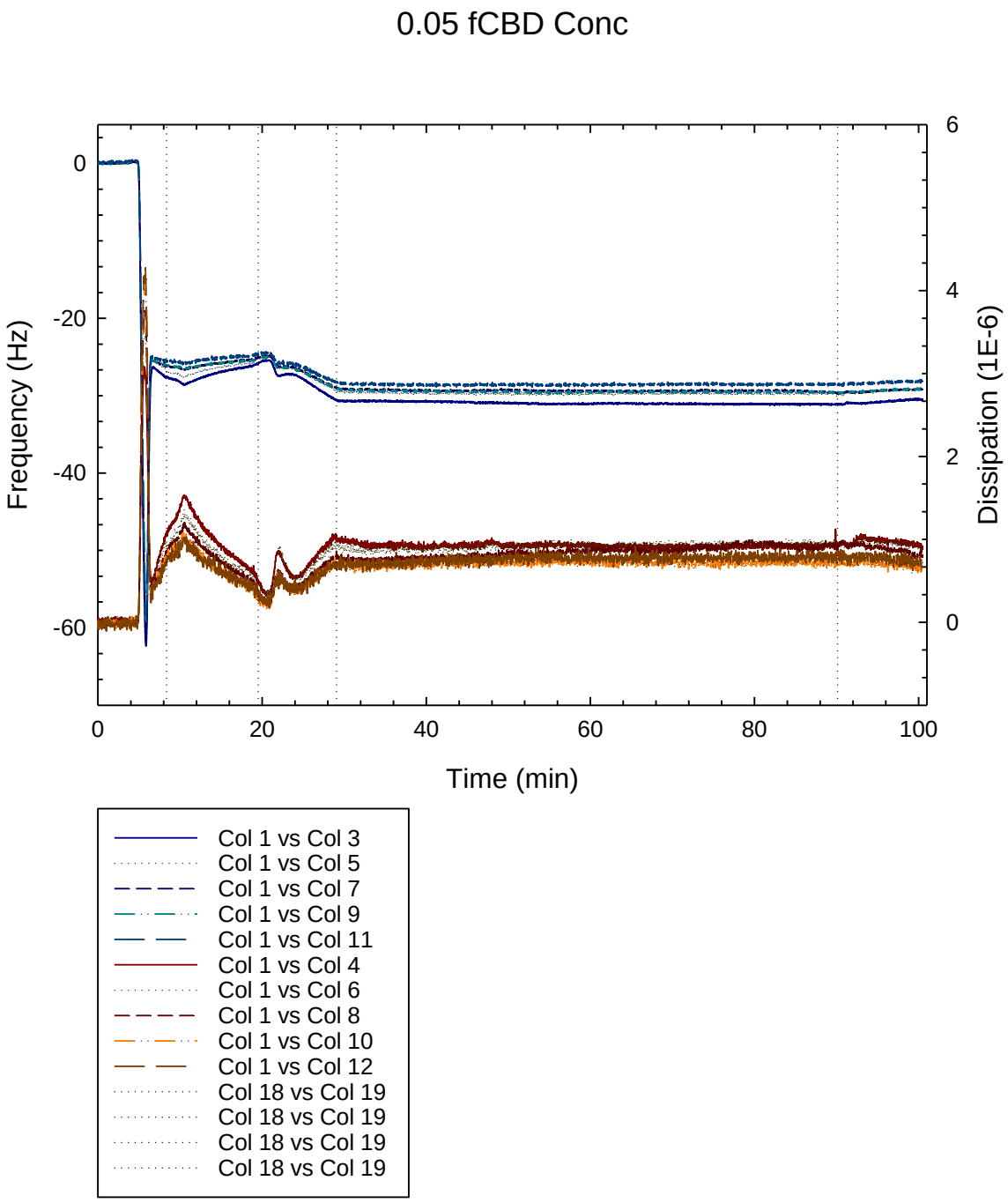

0.05 µM concentration fCBD

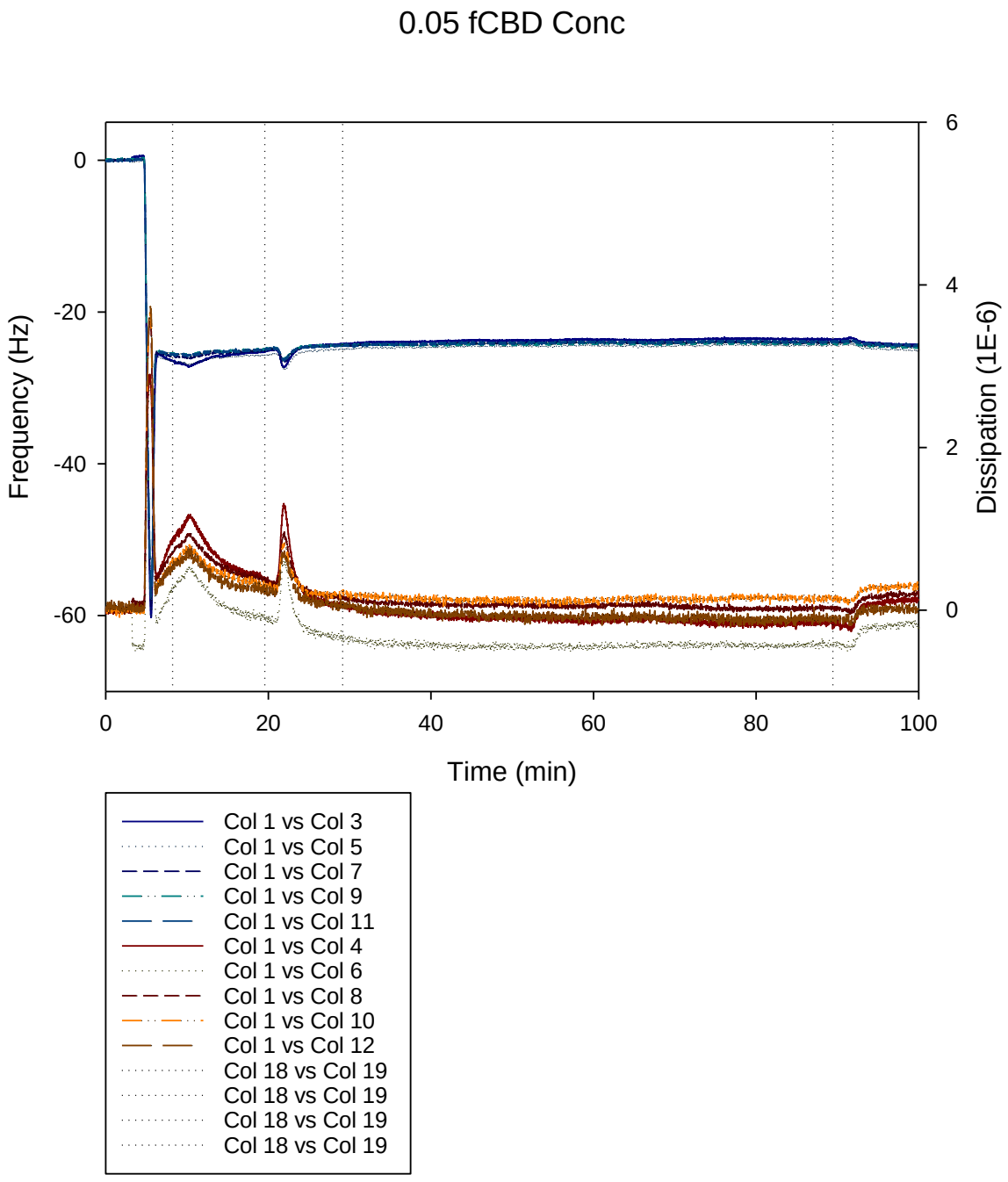

0.05 µM concentration fCBD

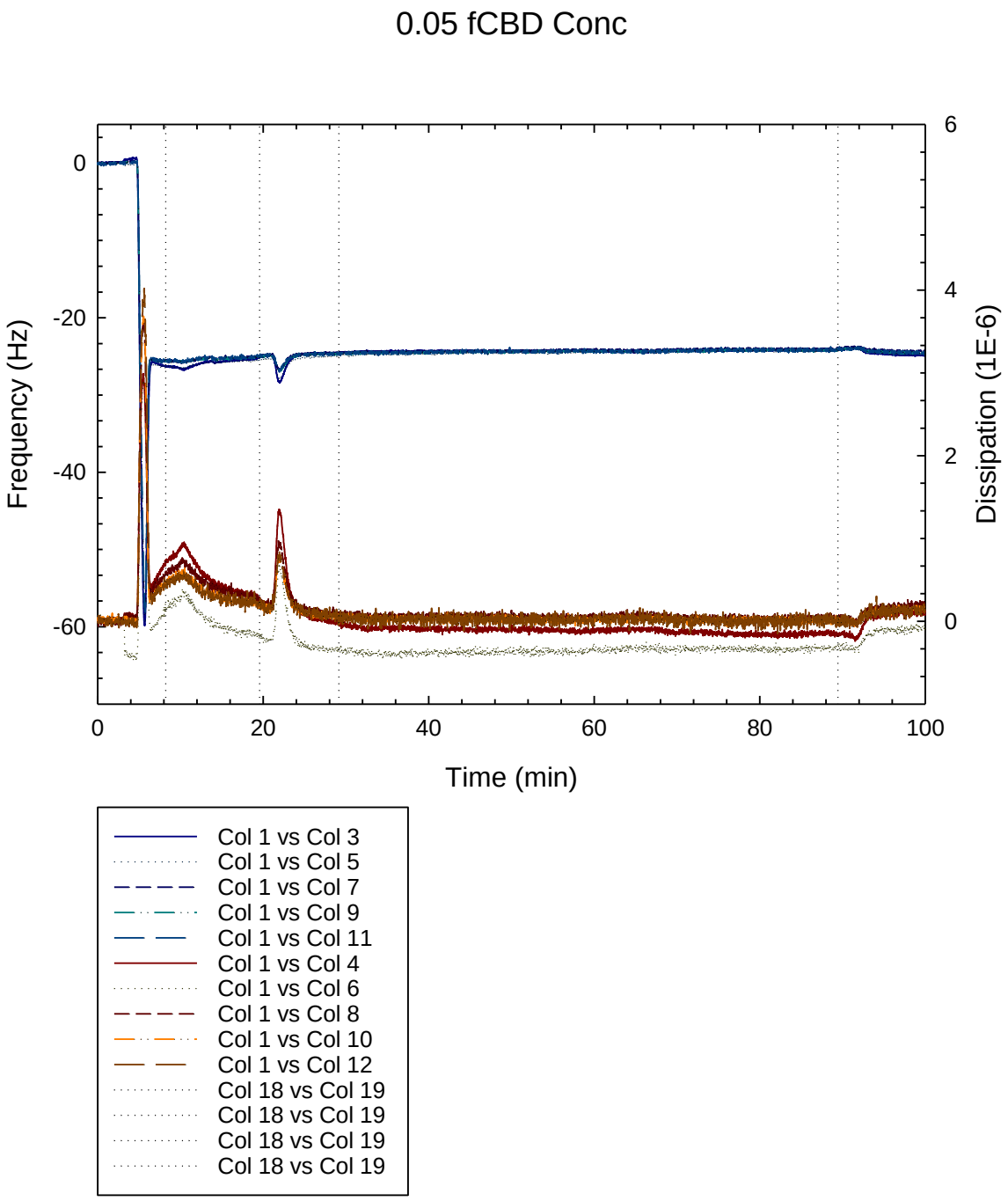

0.1 µM concentration fCBD

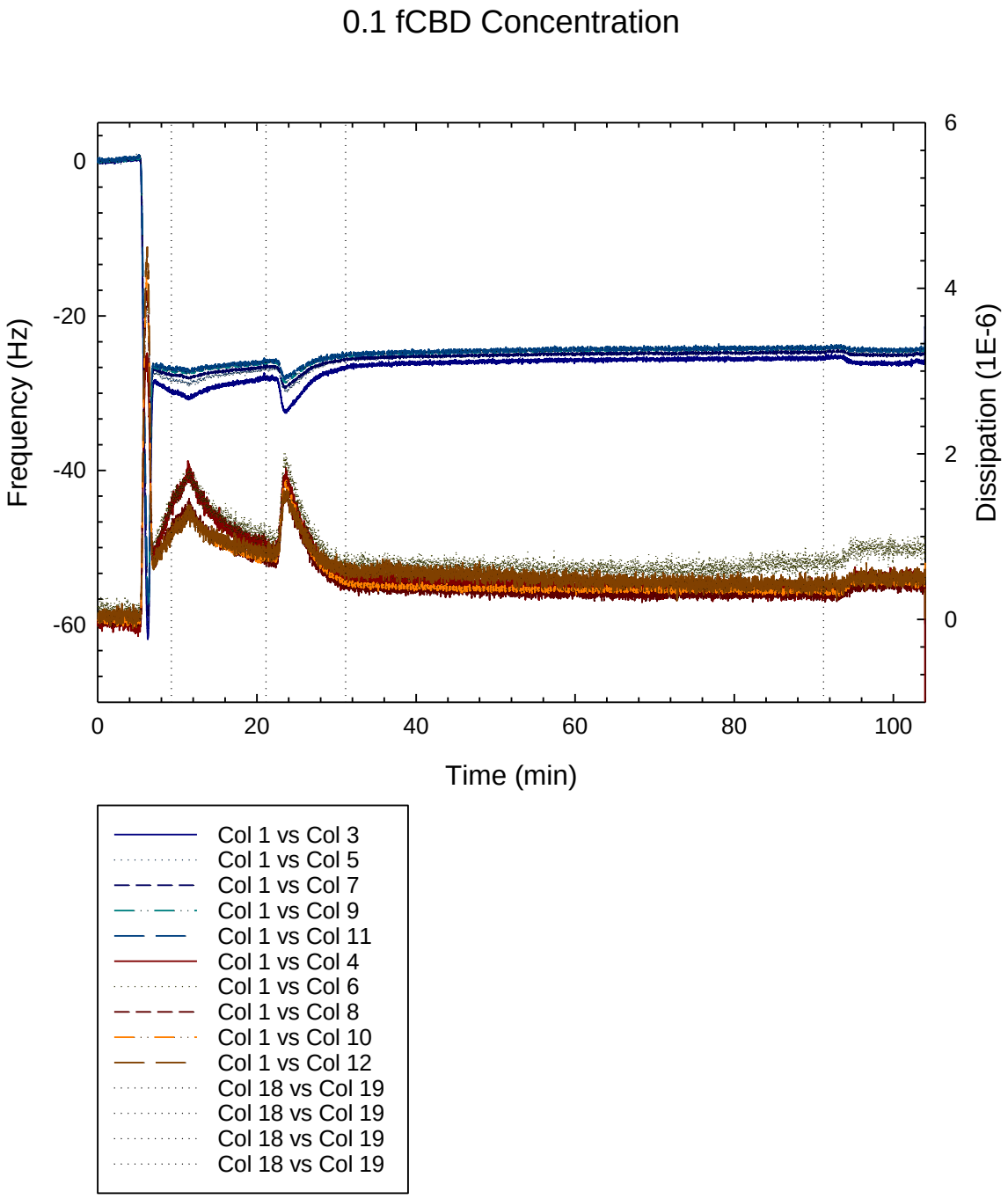

0.1 µM concentration fCBD

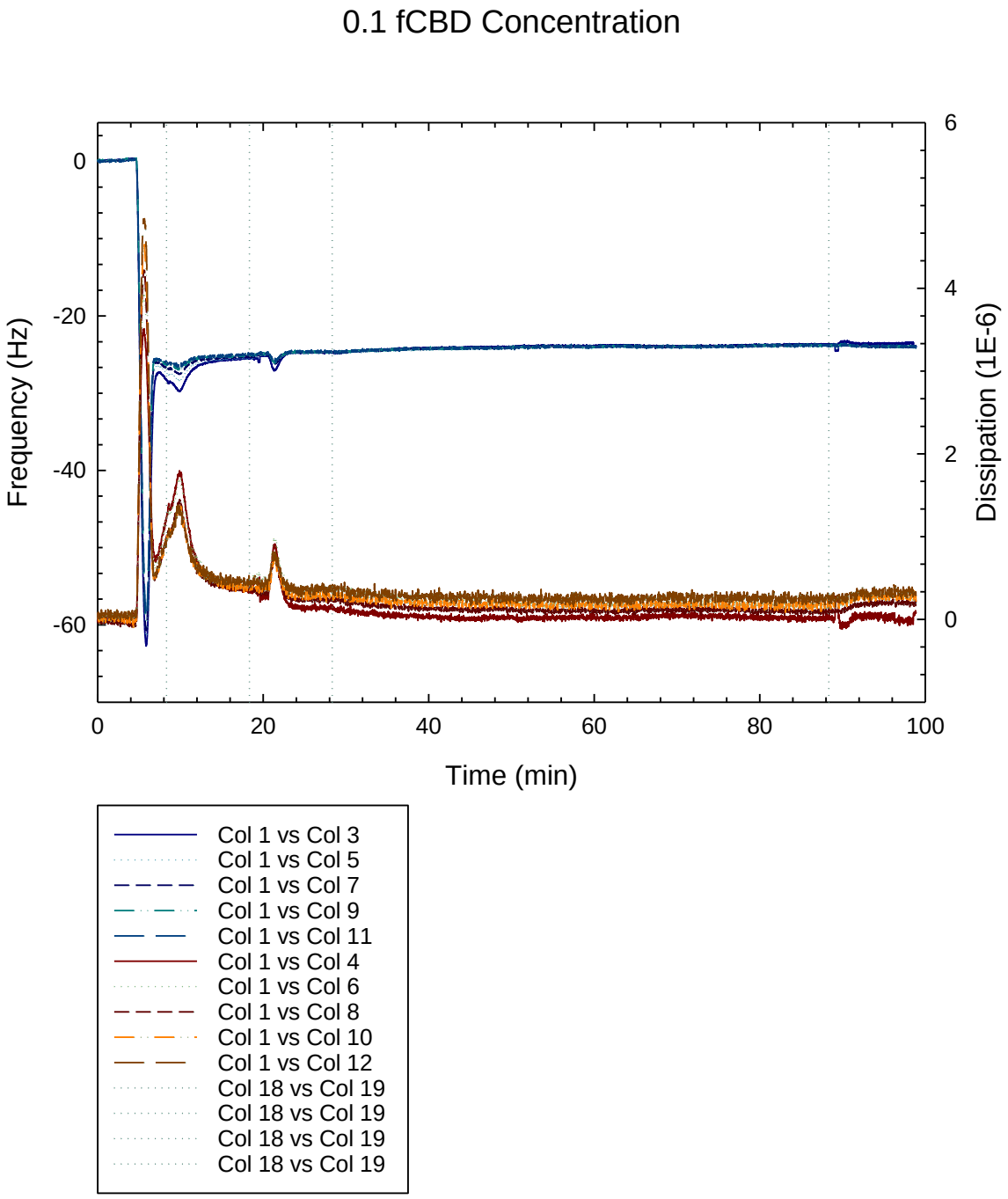

0.1 µM concentration fCBD

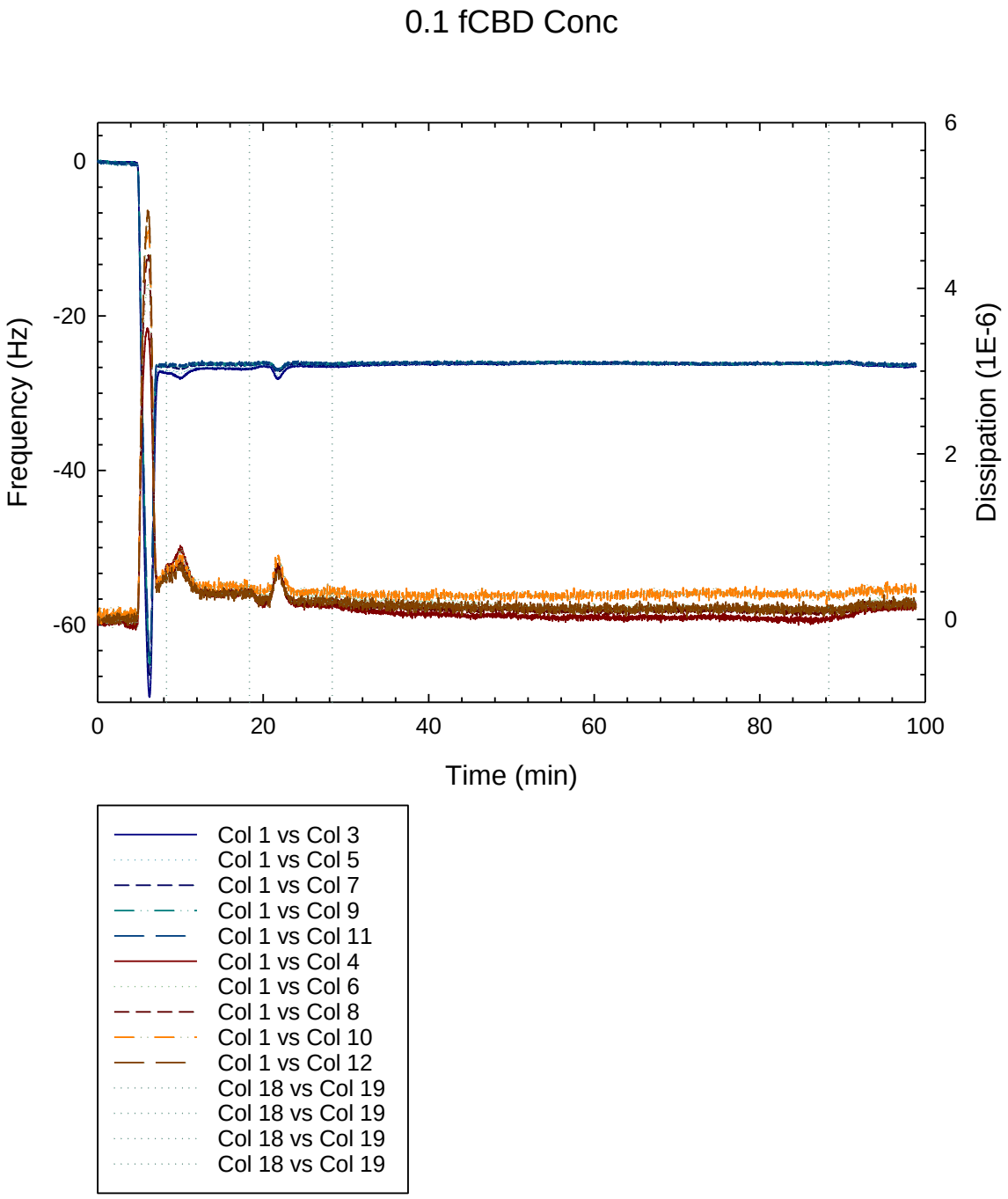

0.25 µM concentration fCBD

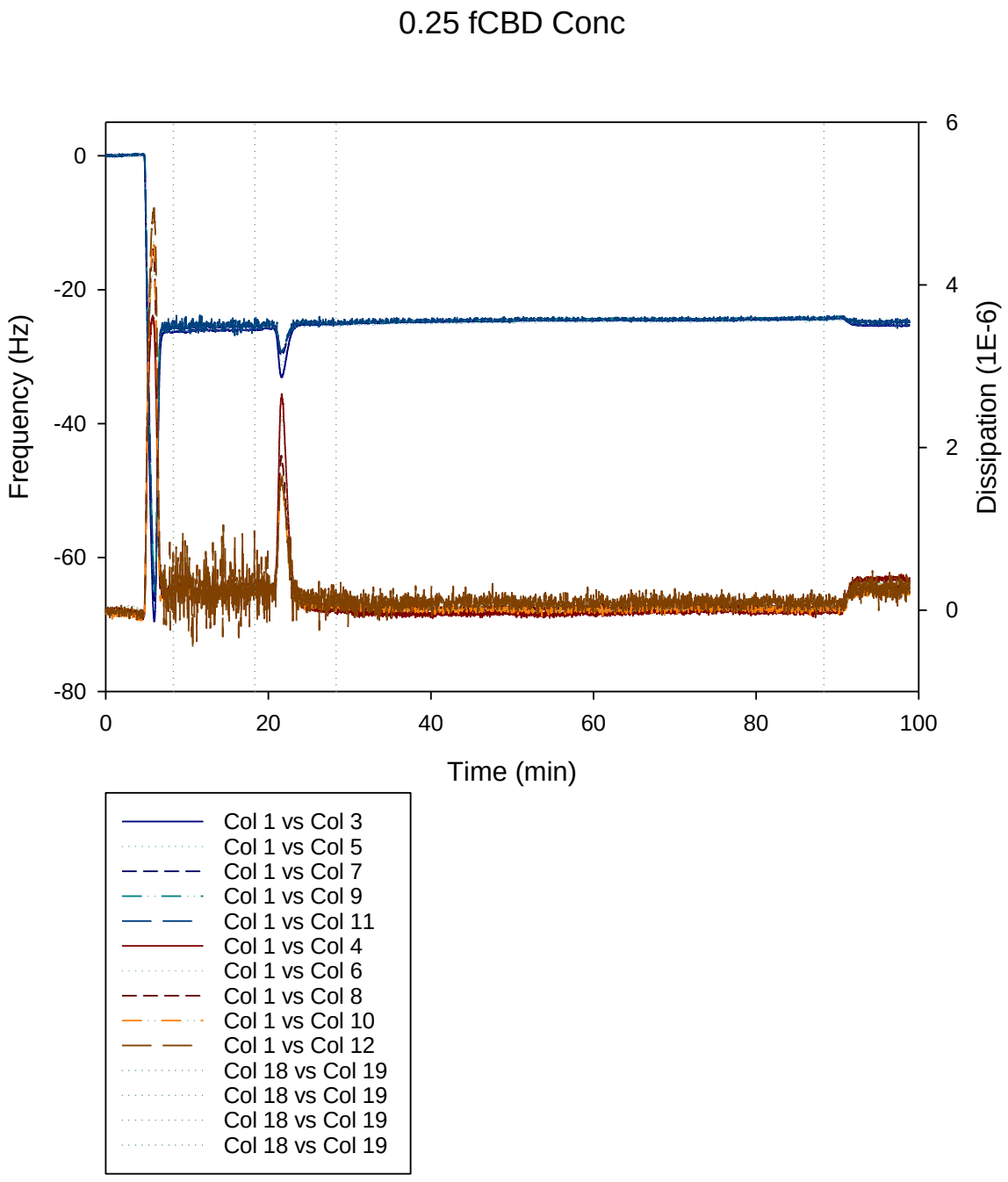

0.25 µM concentration fCBD

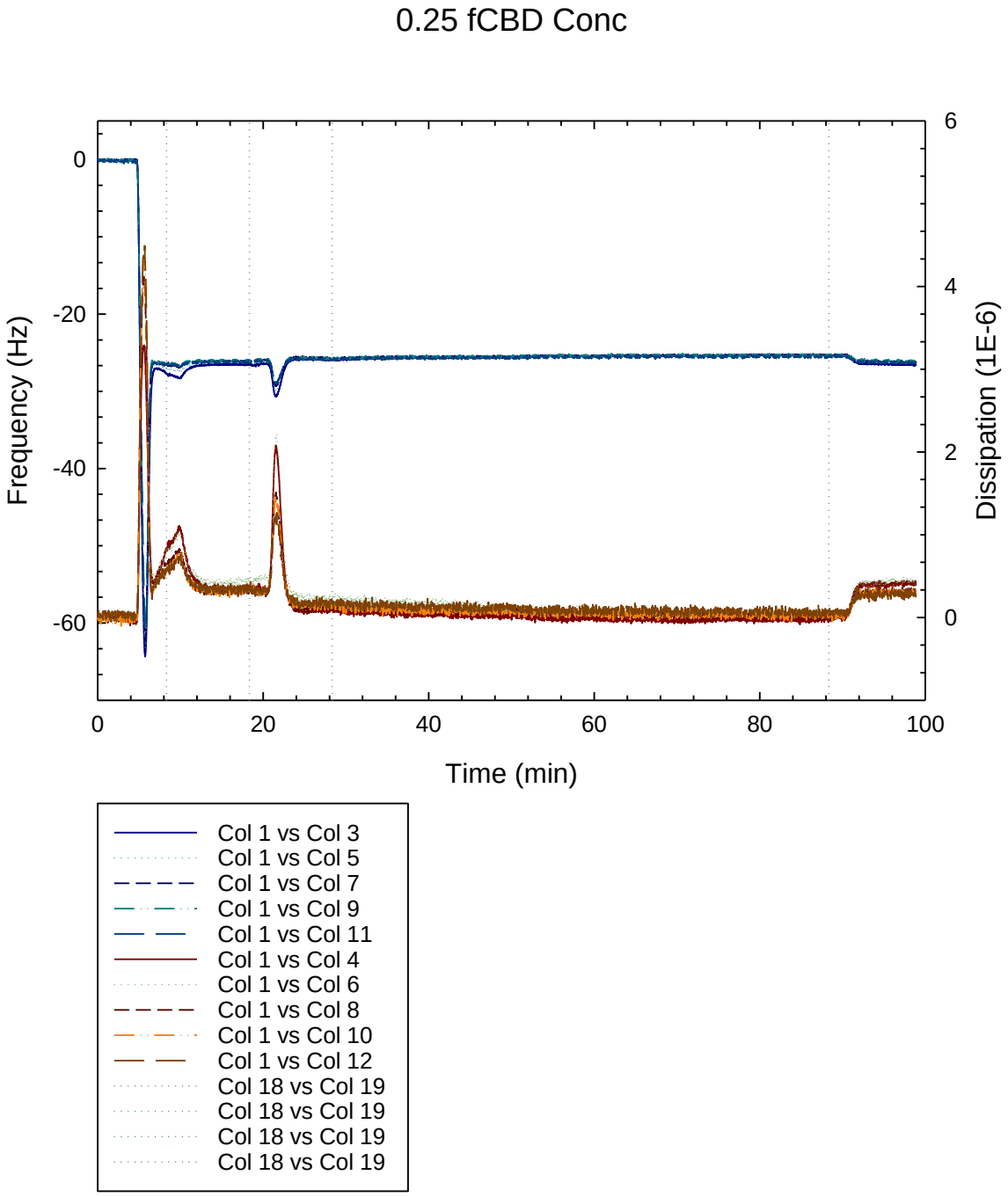

0.25 µM concentration fCBD

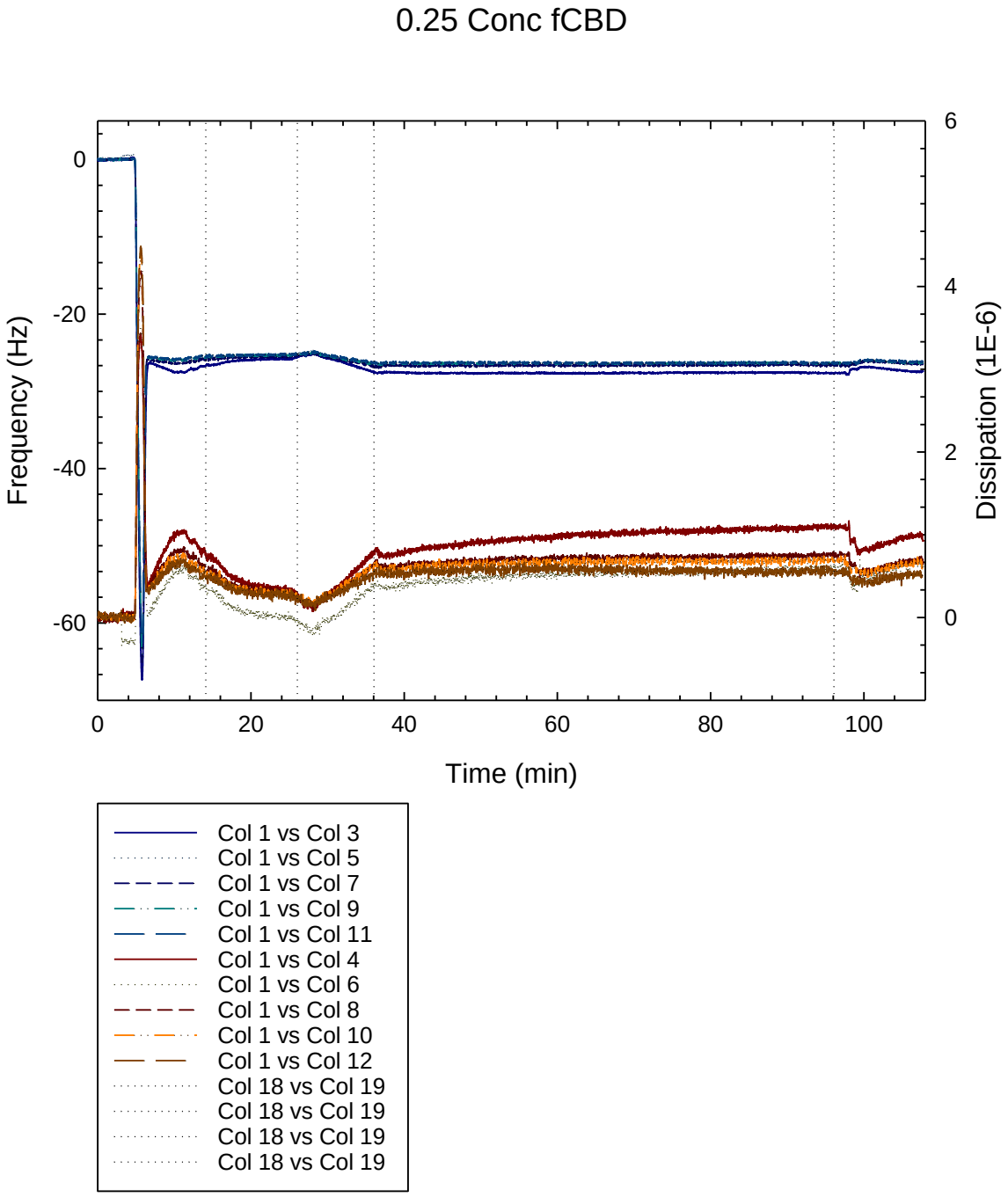

0.25 µM concentration fCBD

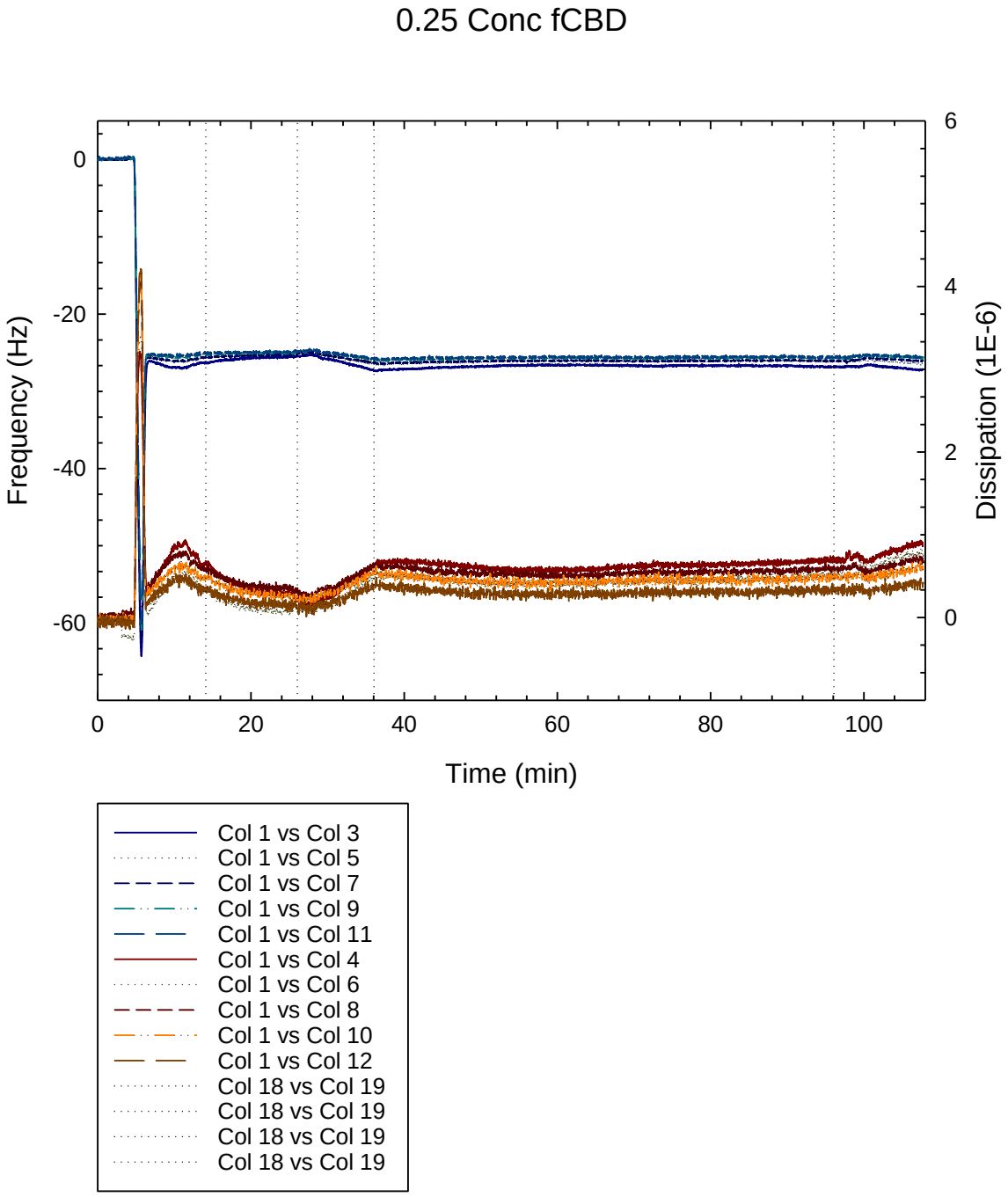

0.5 µM concentration fCBD

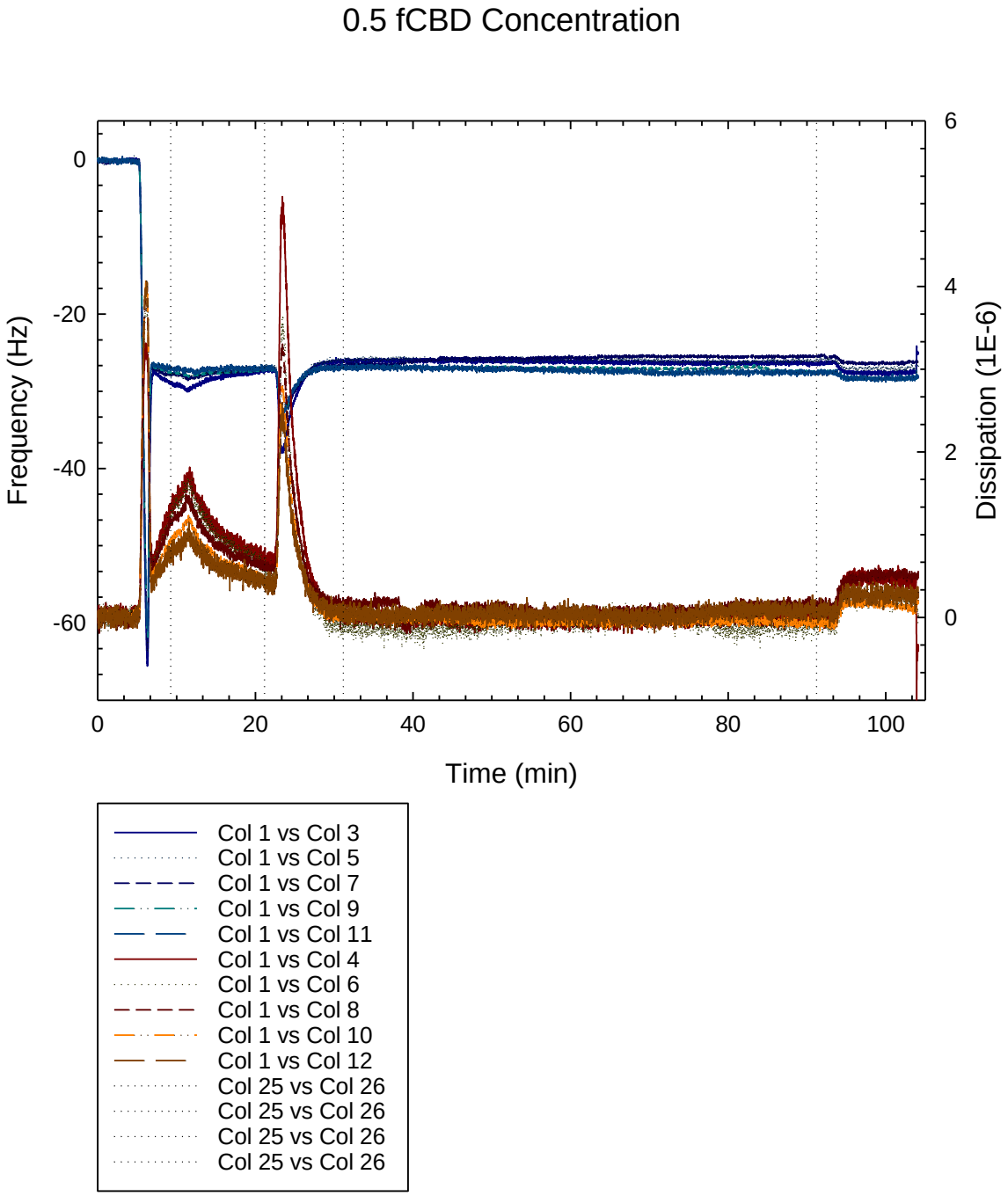

0.5 µM concentration fCBD

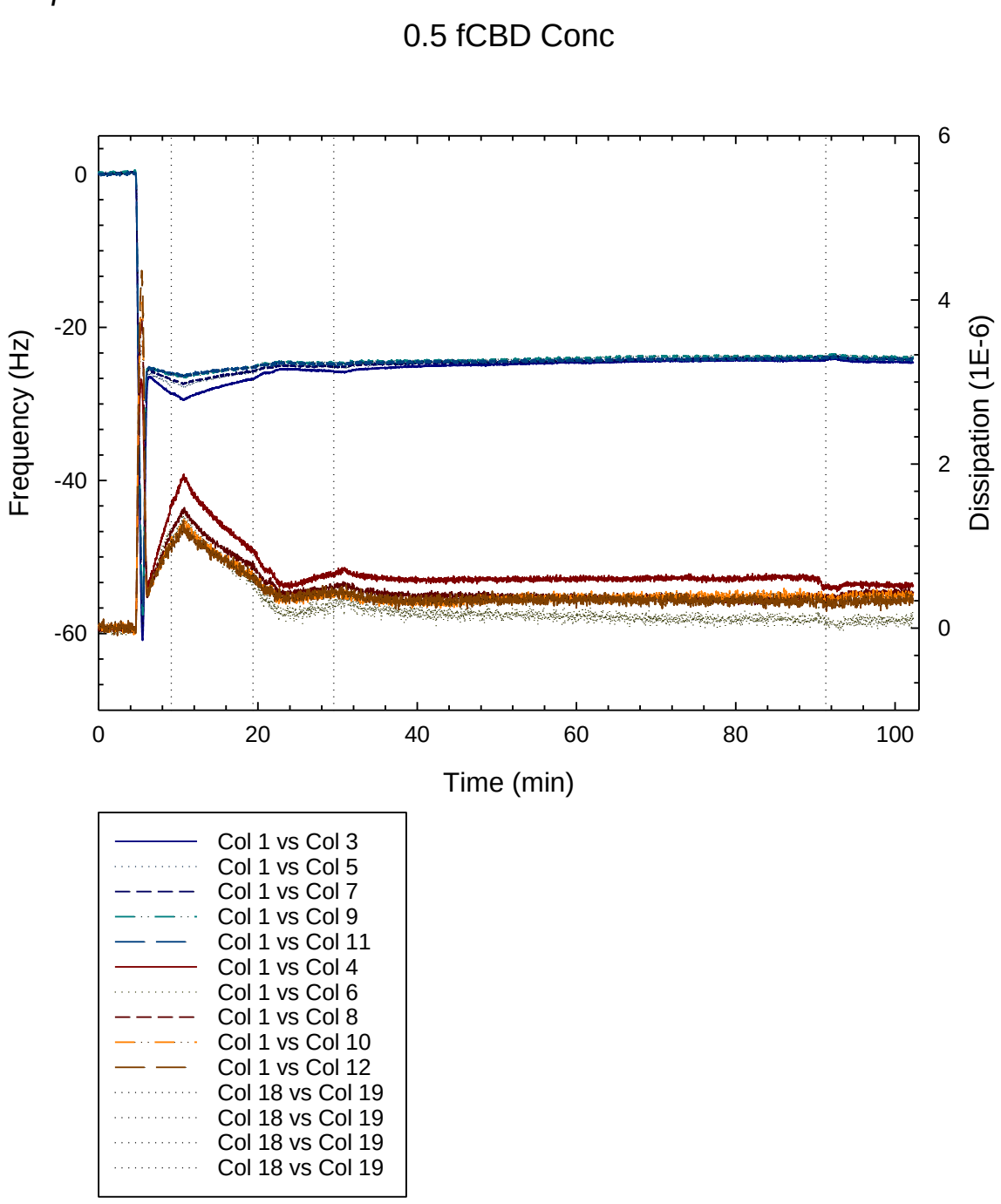

0.5 µM concentration fCBD

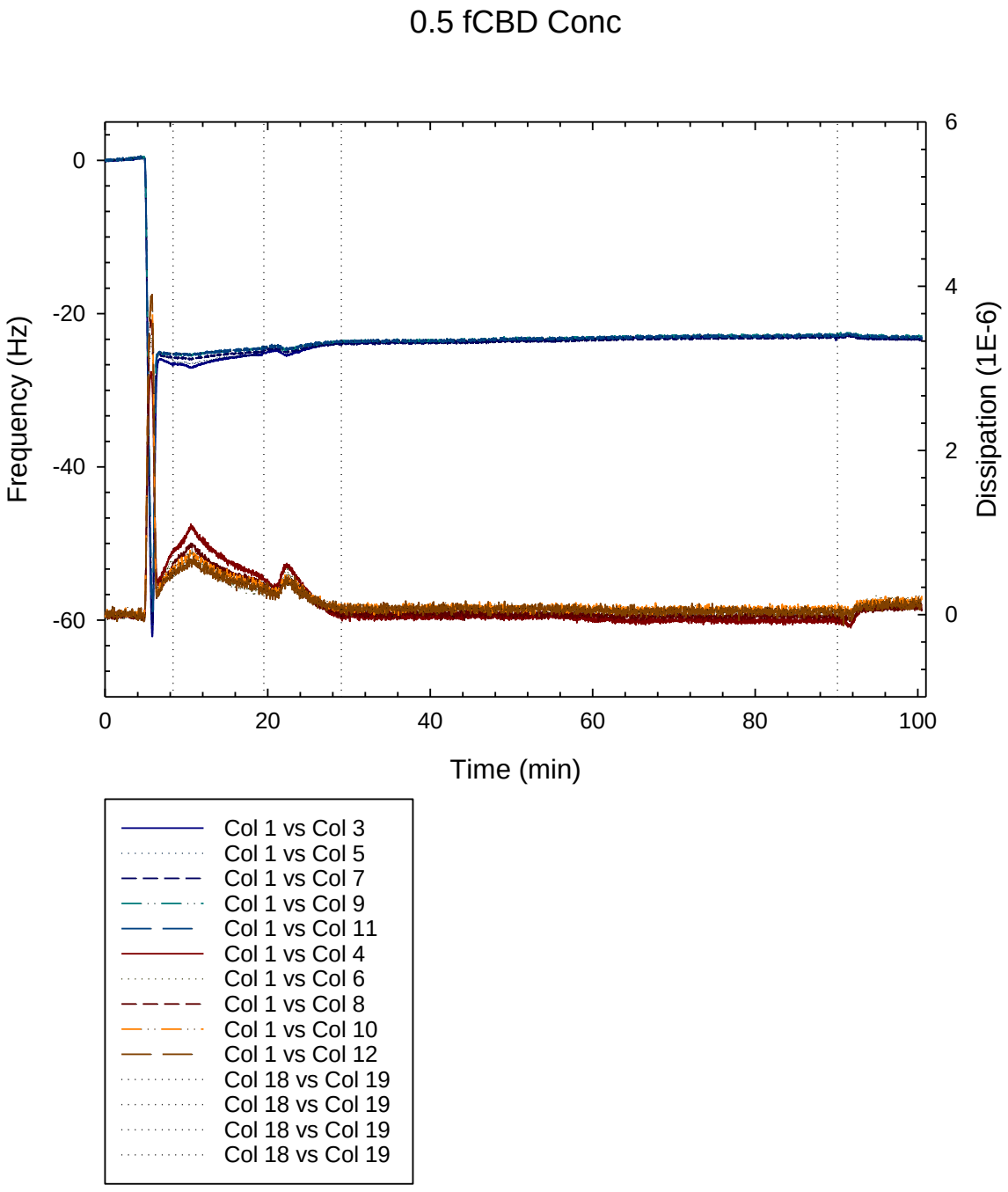

0.5 µM concentration fCBD

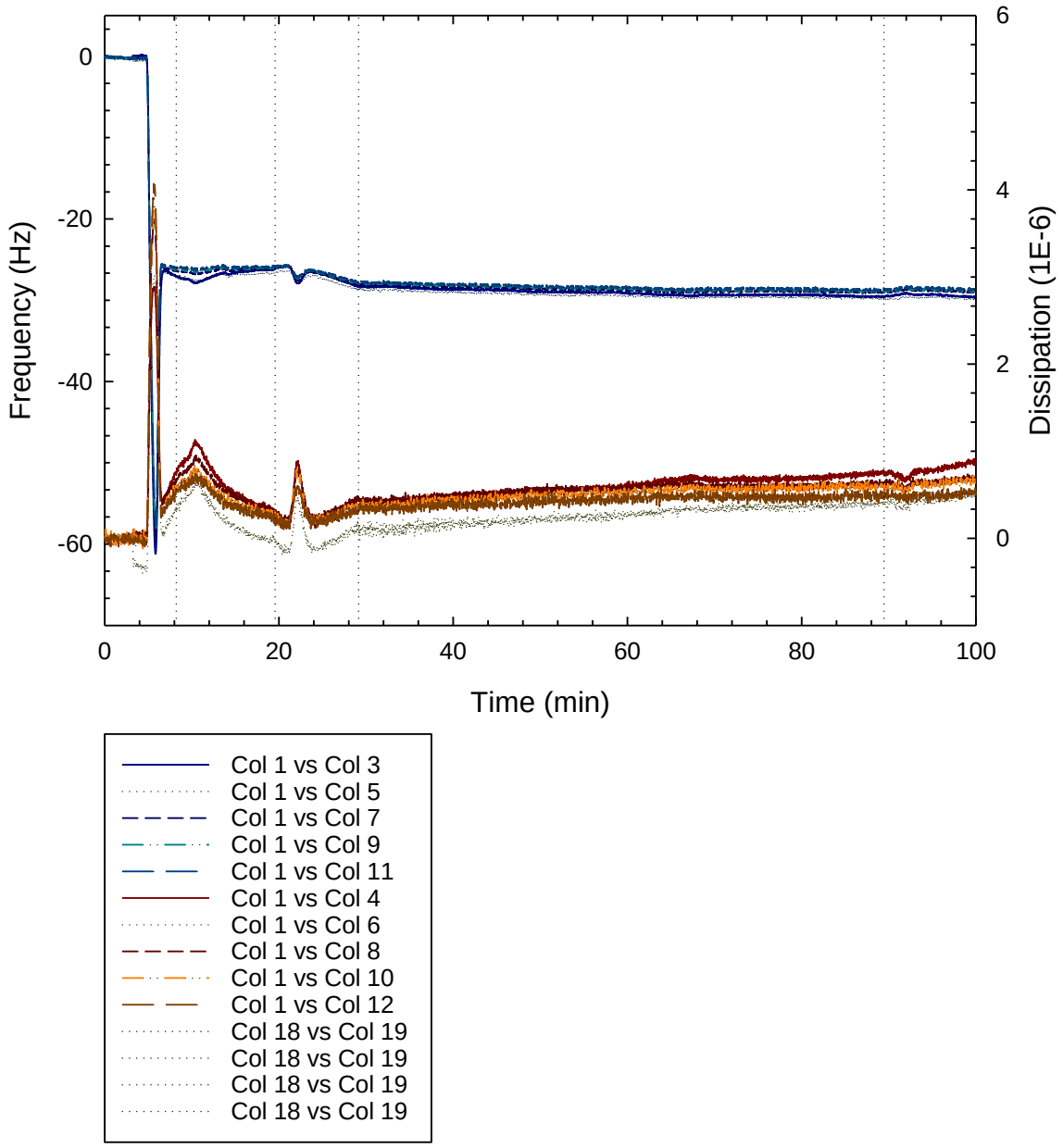

0.5 µM concentration fCBD

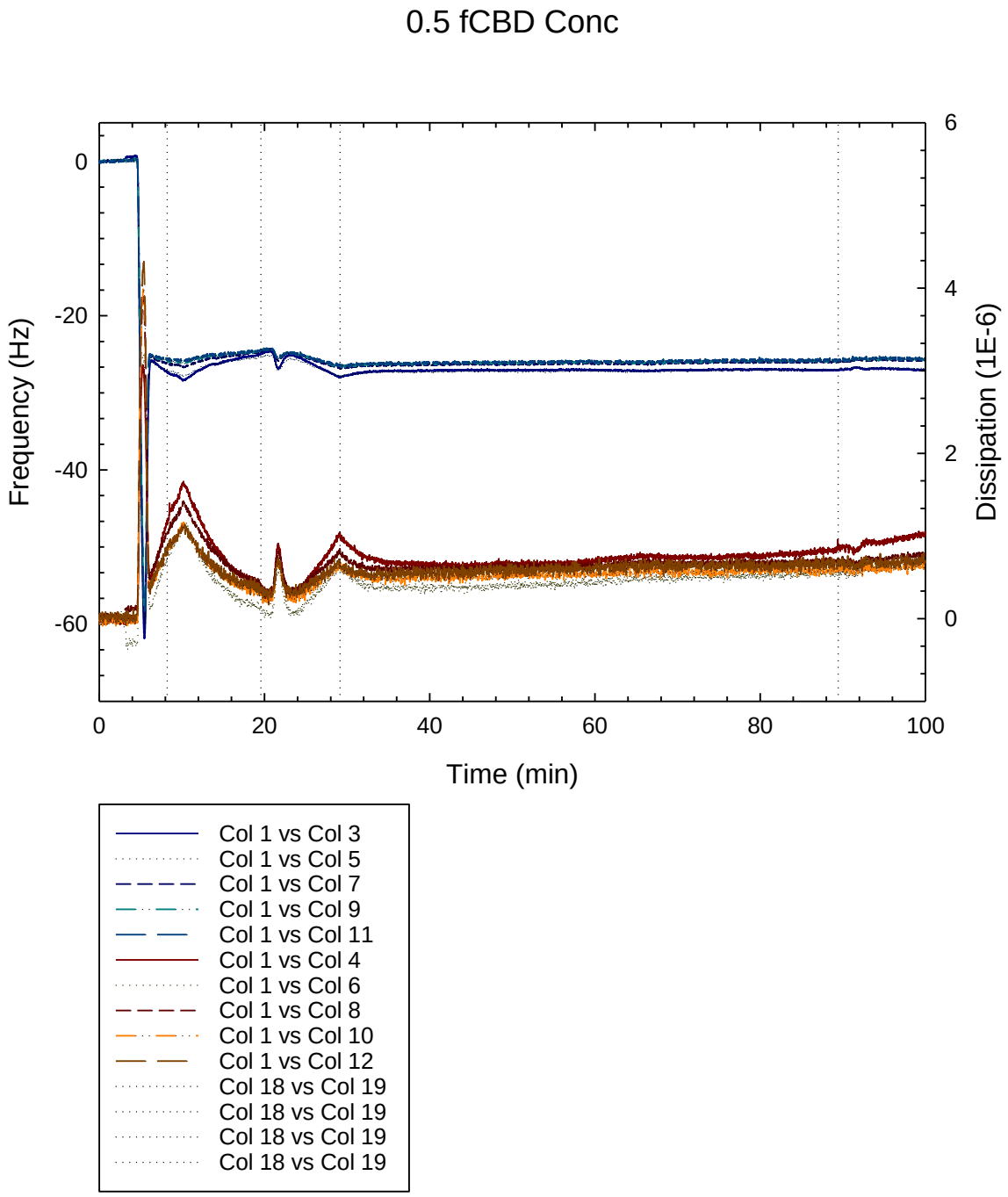

0.5 µM concentration fCBD

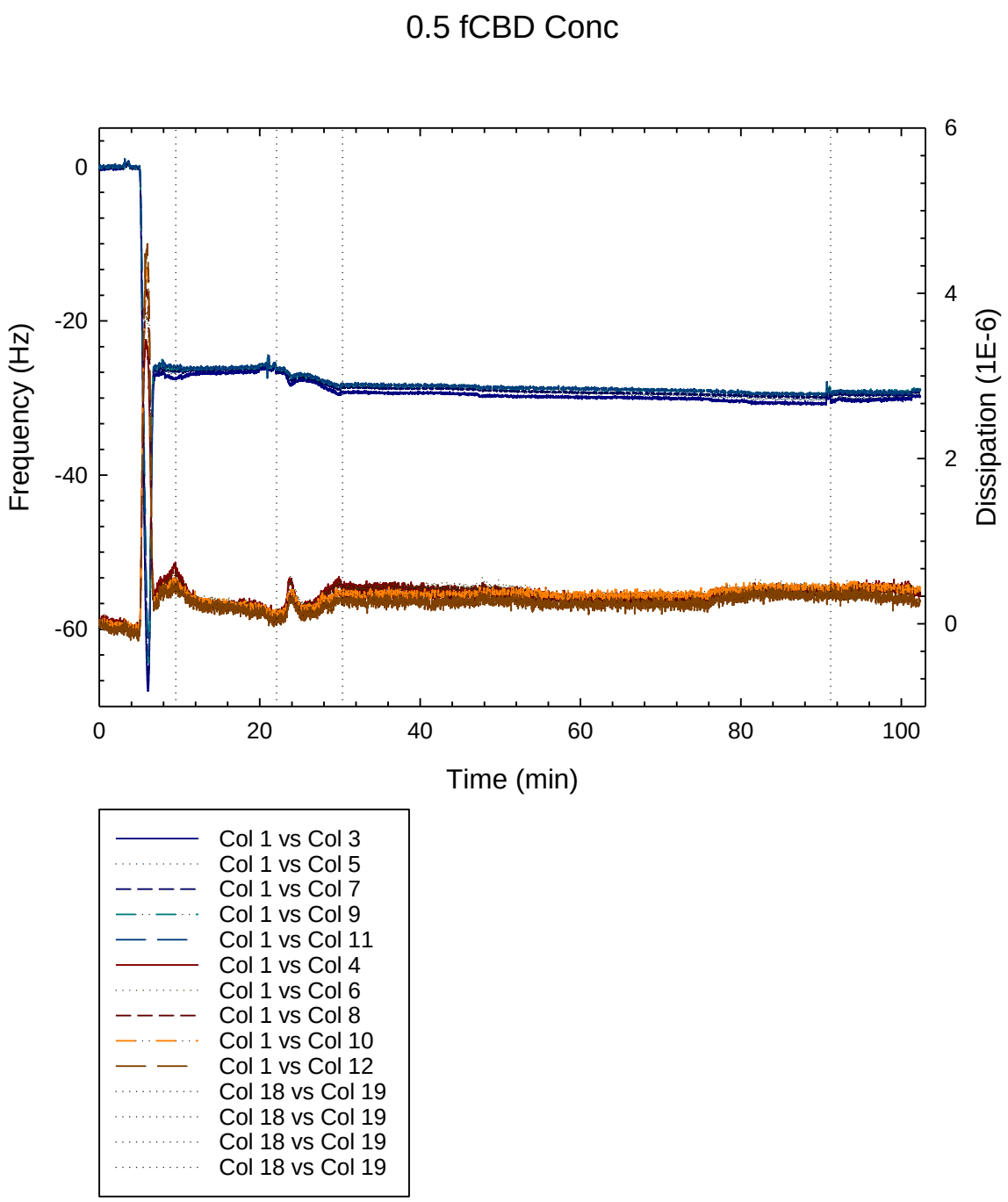

1.0 µM concentration fCBD

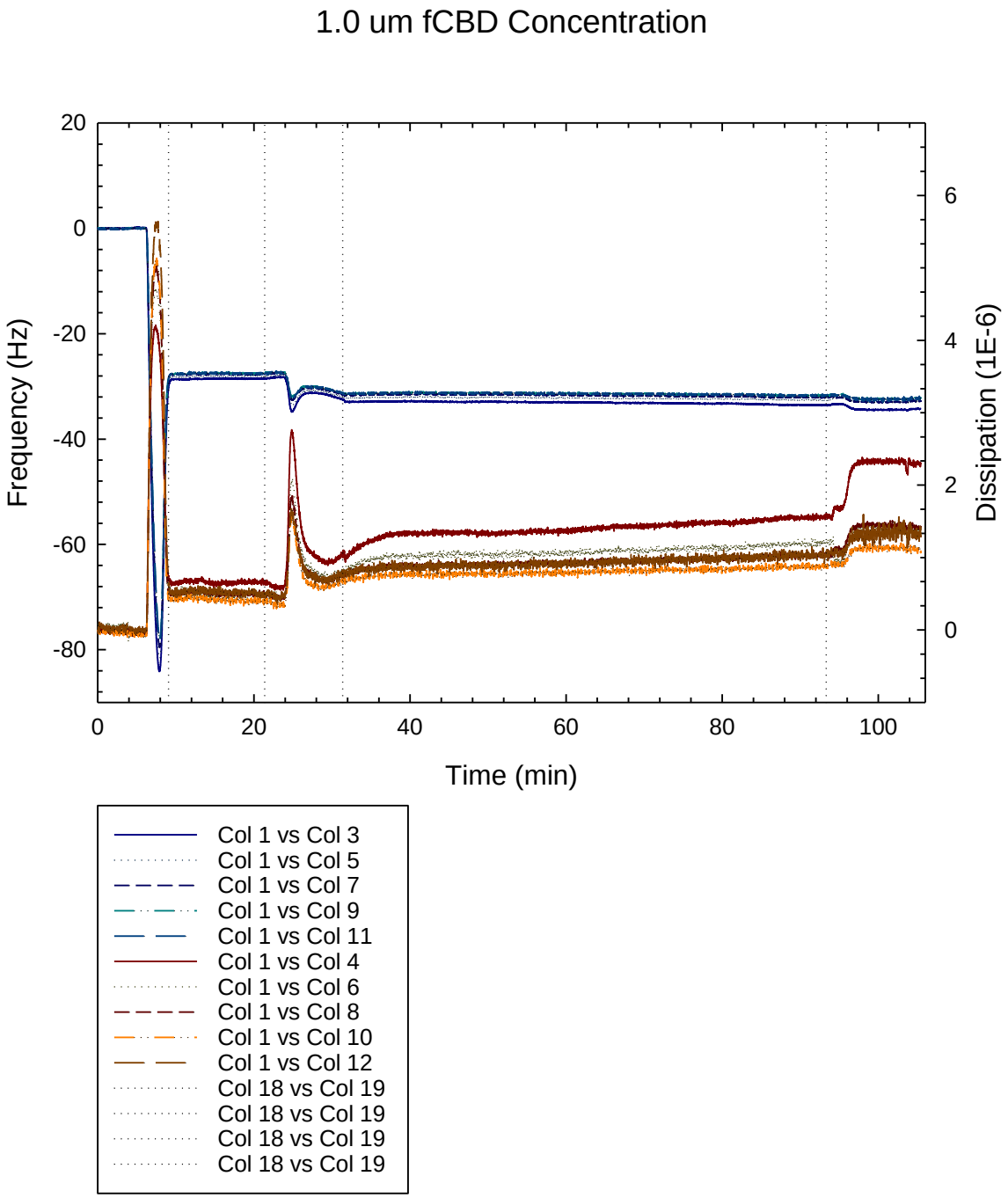

1.0 µM concentration fCBD

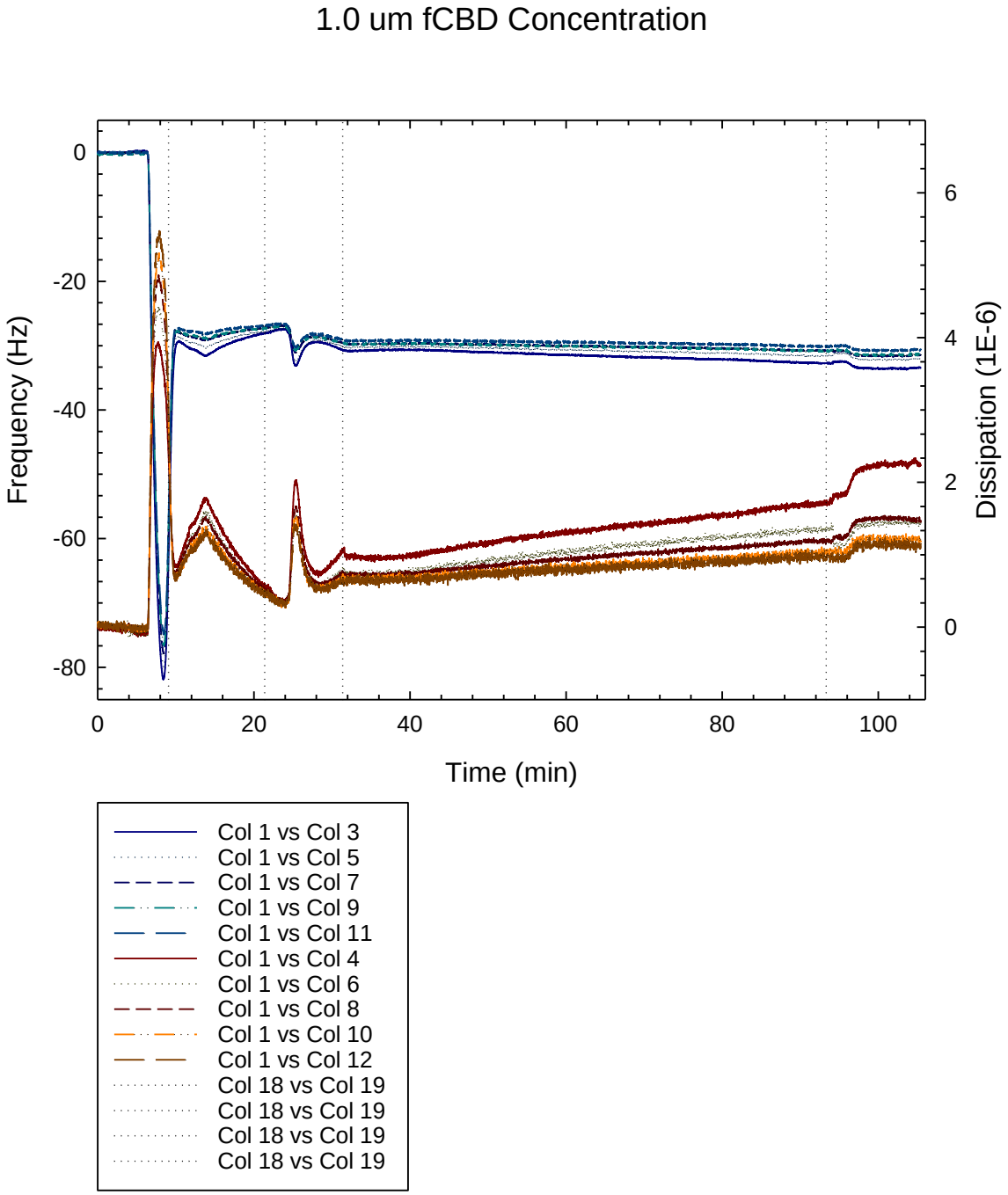

1.0 µM concentration fCBD

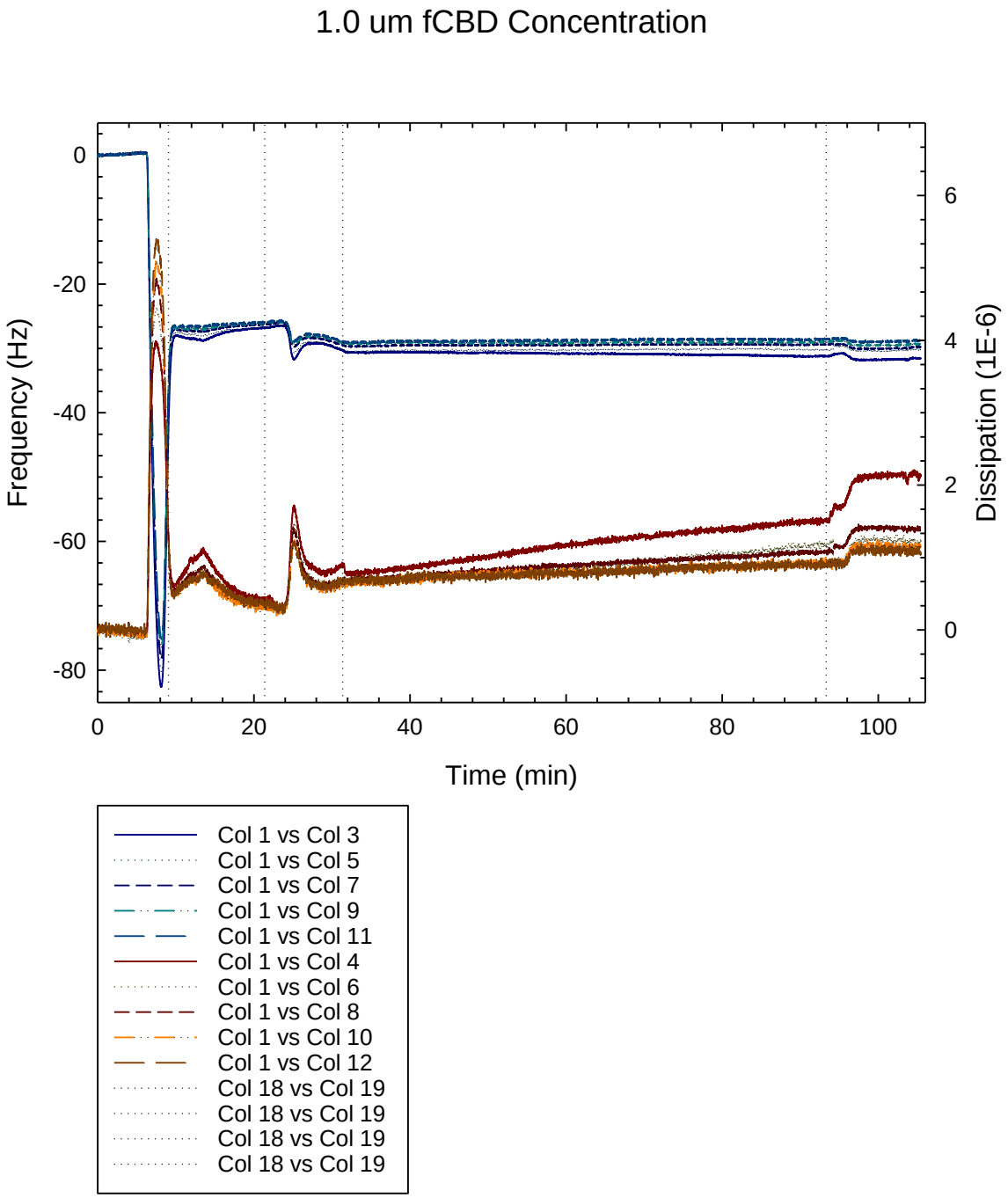

1.0 µM concentration fCBD

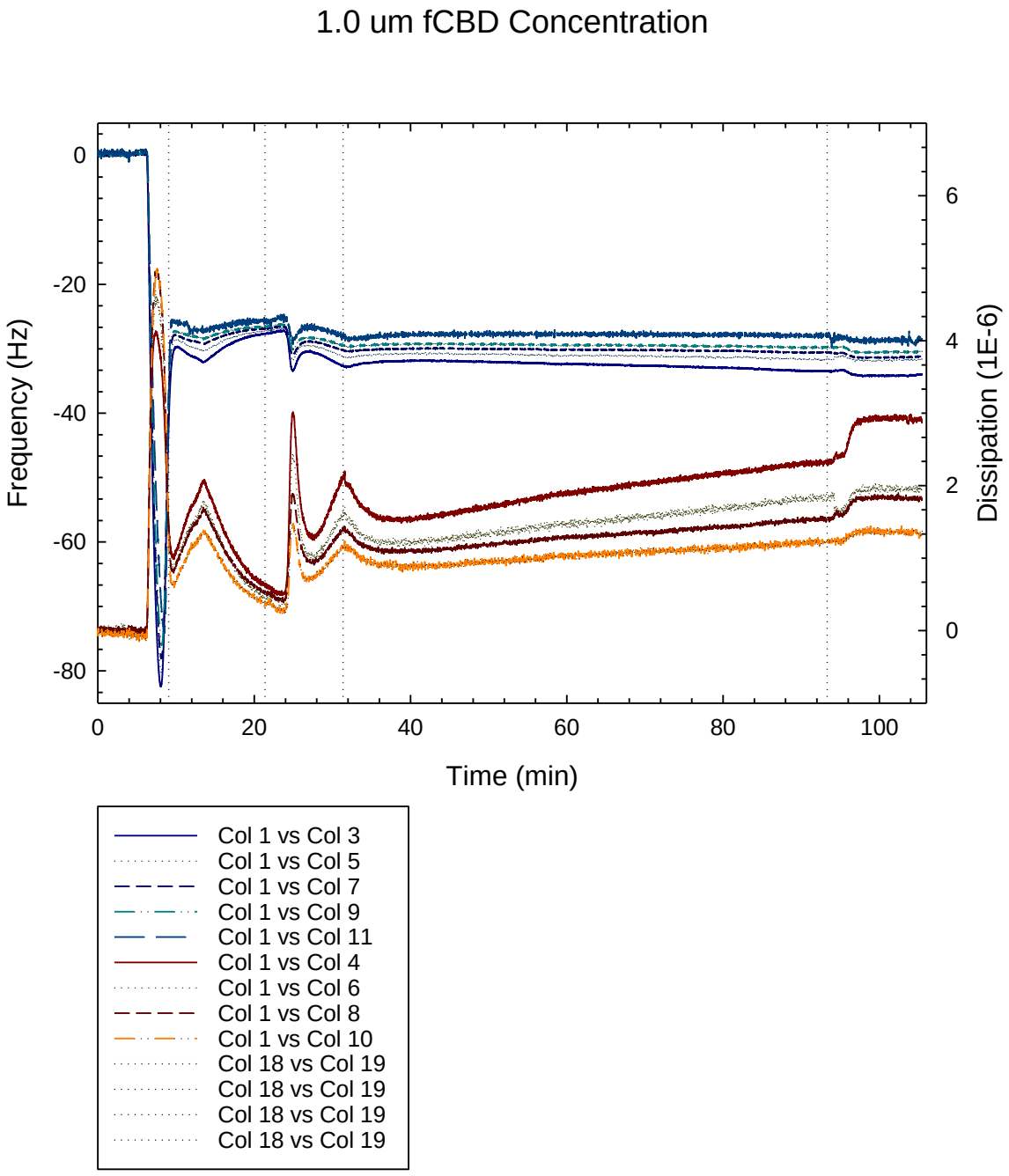

5.0 µM concentration fCBD

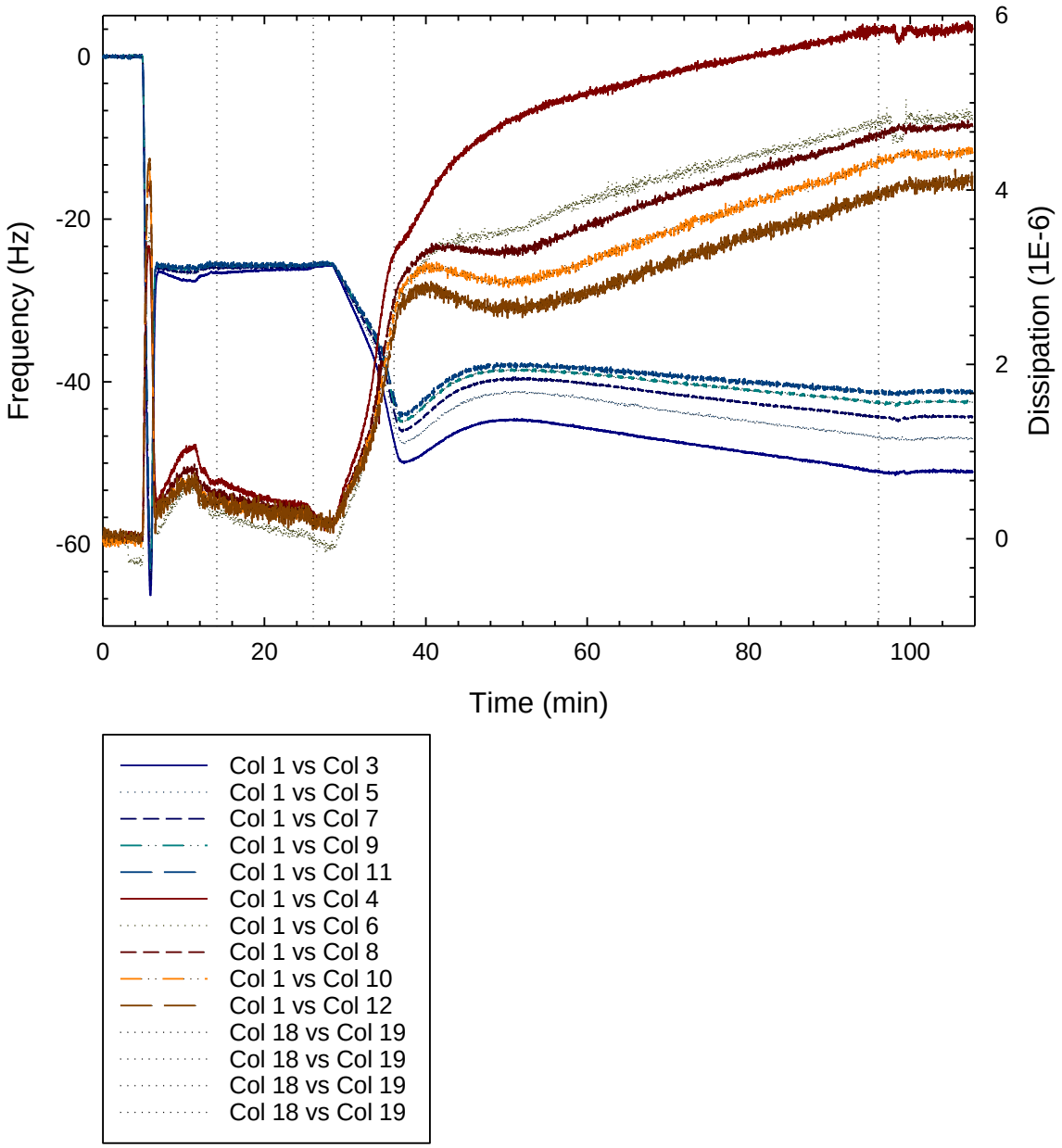

5.0 μM concentration fCBD

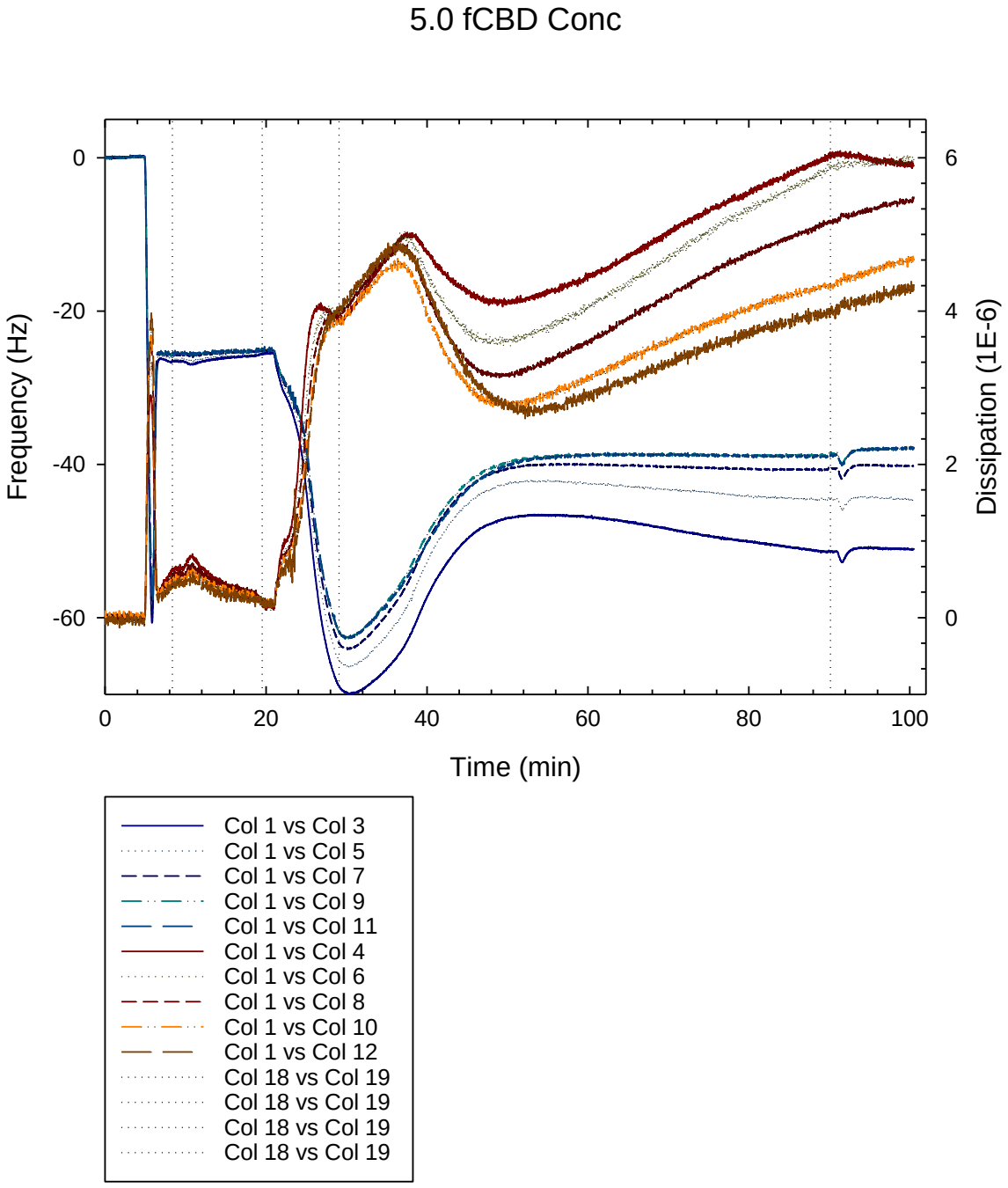

5.0 µM concentration fCBD

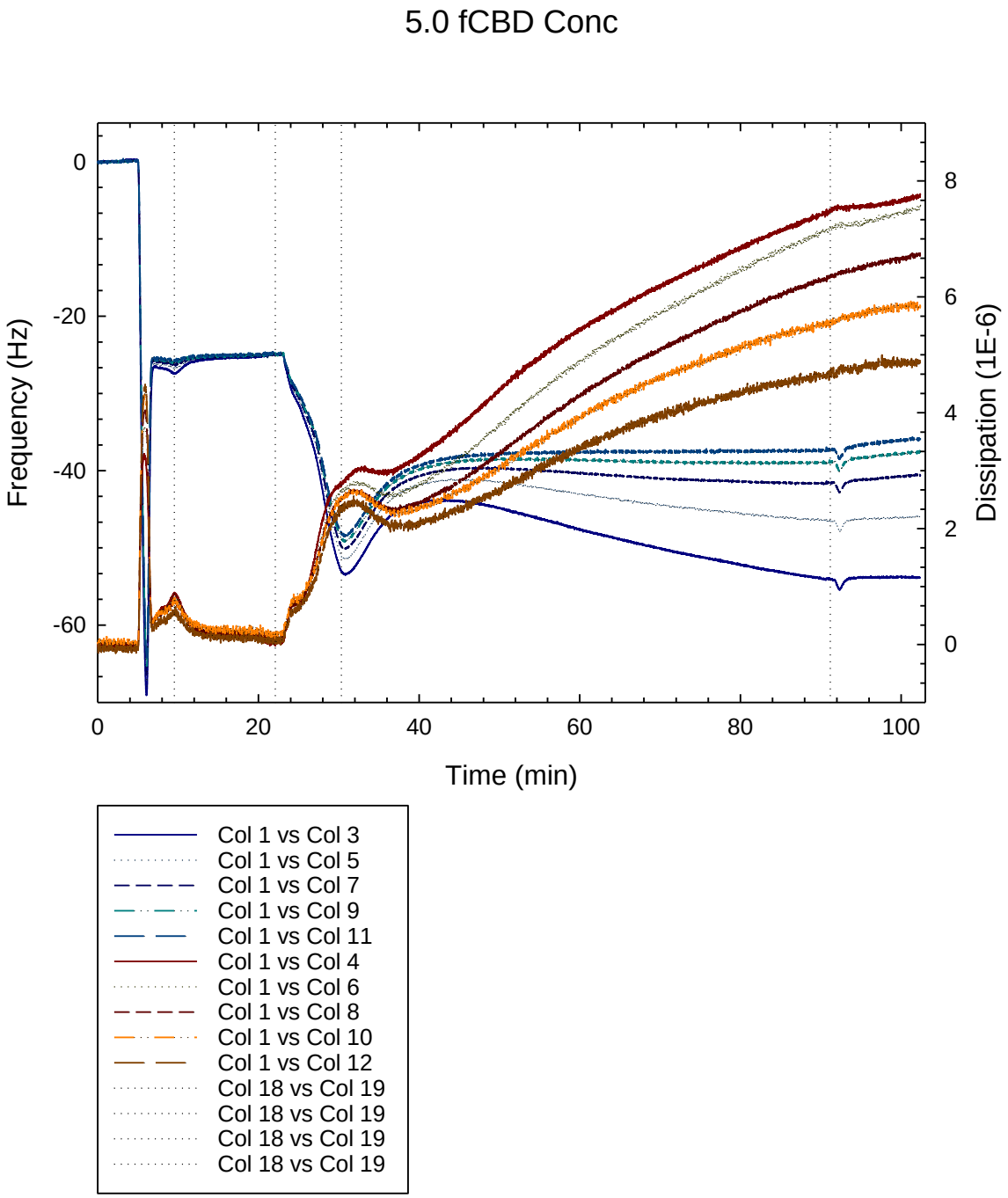

10.0 µM concentration fCBD

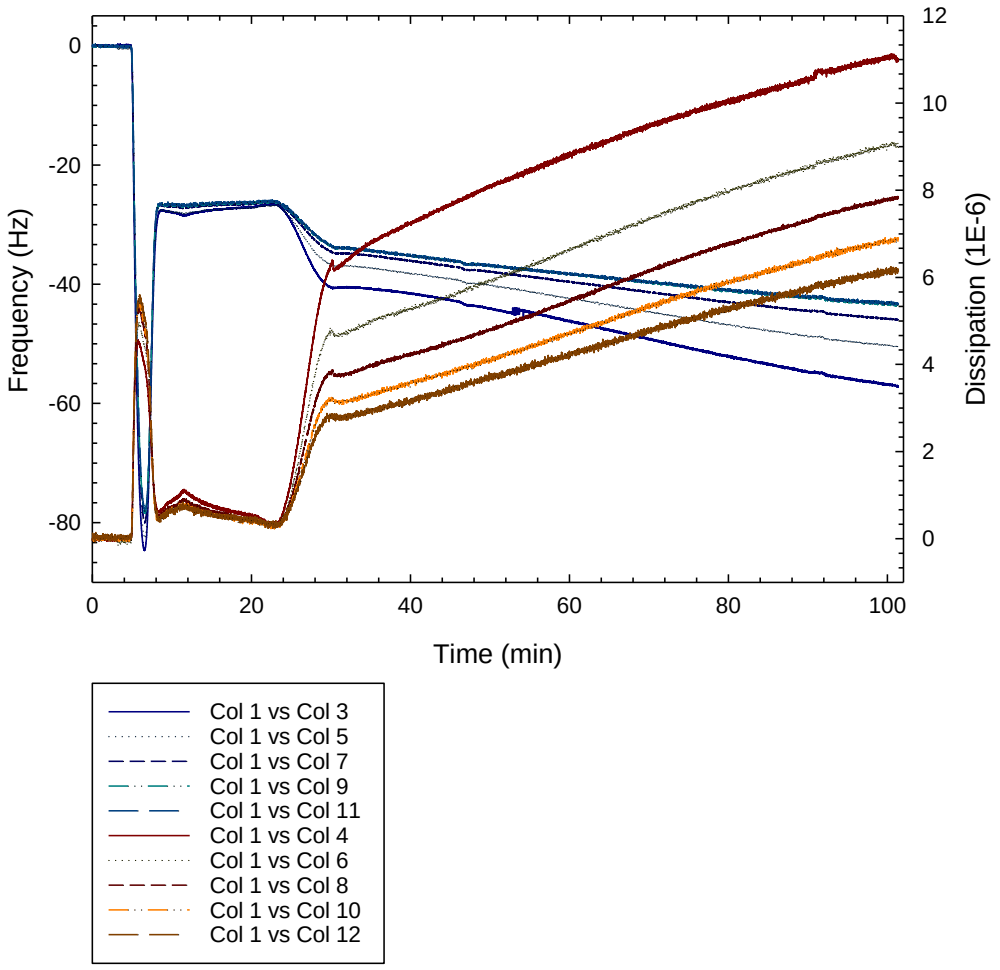

10.0 µM concentration fCBD